Applied Physics B (2026) 132:58
https://doi.org/10.1007/s00340-026-08645-w

Applied Physics B
Lasers and Optics

REVIEW

Roadmap on singular optics and its applications

Ganesh M. Balasubramaniam[1] · Srinivasa Rao Allam[2] · Vijayakumar Anand[3,4] · Md. Haider Ansari[5] · Francis Gracy Arockiaraj[3,6] · Shlomi Arnon[6] · Purnesh Singh Badavath[7] · Mansi Baliyan[21] · Petr Bouchal[8,9] · Zdeněk Bouchal[10] · Sakshi Choudhary[5] · Ahmed H. Dorrah[11] · Yuxiang Duan[12] · Kelsey Everts[13] · Andrew Forbes[13] · Matthew R. Foreman[1,14] · Darius Gailevičius[15] · Akanksha Gautam[16] · Greg Gbur[17] · Shivasubramanian Gopinath[3] · Narmada Joshi[3] · Saulius Juodkazis[4,18] · Olga Korotkova[19] · Kaupo Kukli[3] · Judy Kupferman[6] · Praveen Kumar[20] · Ravi Kumar[5] · Vijay Kumar[7] · Gokul Manavalan[6] · Ayush Mehra[6] · Naveen K. Nishchal[21] · Takashige Omatsu[2,26,27] · Cade Peters[13] · Andra Naresh Kumar Reddy[22,23] · Salla Gangi Reddy[5] · Valeria Rodríguez-Fajardo[24] · Carmelo Rosales-Guzmán[25] · Joseph Rosen[6] · Sarita[16] · Allarakha Shikder[21] · Rakesh Kumar Singh[16] · Xinzhou Su[12] · Aile Tamm[3] · Ganesh Velagala[5] · Petr Viewegh[8,9] · Eulàlia Puig Vilardell[3,4,18] · Alan E. Willner[12] · Agnes Pristy Ignatius Xavier[6] · Amit Yadav[16] · Huibin Zhou[12]

Received: 20 December 2025 / Accepted: 10 February 2026 / Published online: 8 April 2026

Abstract
Singular optics is a branch of modern electromagnetics and optics that investigates solutions to Maxwell's equations that exhibit nontrivial topological features under various boundary conditions. These solutions give rise to light fields containing singularities, points or regions at which certain optical properties, such as phase or polarization, become undefined. Over time, singular optics has evolved into a unifying framework for understanding and engineering optical fields that possess phase, polarization, coherence, and spatiotemporal singularities, each characterized by quantized topological properties. Such structured light fields enable high-dimensional information encoding, robust light–matter interactions, and sensitive probing of complex media, thereby impacting optical communication, imaging, sensing, and materials processing. Parallel advances in theory, fabrication techniques, detection hardware, and computational methods have created a diverse and rapidly expanding landscape, underscoring the need for an integrated and forward-looking perspective. This roadmap synthesizes emerging applications of singular optics across multiple platforms, offering a concise overview of current developments and highlighting key physical concepts, new architectures, and transformative technologies that bridge subfields. In addition to reflecting the insights of leading contributors to these research directions, it also surveys selected recent advances, providing a concise overview of current trends and a foundation for shaping the future of singular optics and its applications.

1 Introduction (Ganesh M. Balasubramaniam and Shlomi Arnon)

Singular optics studies optical fields whose phase, amplitude, polarization, or coherence exhibit regions where these quantities are undefined or change discontinuously. Such singular structures emerge naturally from solutions of Maxwell's equations and possess a well-defined topological character, including integer phase winding and defects in the polarization field. Because these features are quantized and robust under perturbations, singular optics provides a rigorous framework for analysing and engineering structured light with tailored phase, polarization, and spatiotemporal properties. The systematic analysis of such wave dislocations by Nye and Berry showed that these defects carry conserved topological charges and follow robust geometrical and statistical rules that are largely independent of the underlying implementation [1]. Subsequent work established singular optics as a distinct branch of physical optics that unifies phase and polarization singularities within a common topological framework [2–4].

Extended author information available on the last page of the article

Over the past decades this viewpoint has transformed how complex optical fields are described and engineered. Singular structures now include scalar optical vortices that carry orbital angular momentum, vector beams with spatially varying polarization, coherence and correlation singularities, and spatiotemporal vortices in pulsed fields [2, 3, 5–7]. These objects provide a natural language for modern sources and devices that sculpt light in amplitude, phase, polarization, and time, using spatial light modulators, nanophotonic elements, and metasurfaces.

At the same time singularities have evolved from mathematical curiosities into practical resources. Structured beams with well defined singularities enable high dimensional information encoding and multiplexing, resilient free- space and guided wave communication, and tailored light–matter interaction in both linear and nonlinear regimes [6, 8–12]. Singular structures also emerge naturally in random and partially coherent fields, in nonlinear frequency conversion, and in topological and non Hermitian photonic platforms. As a result singular optics now links communities that span classical and quantum optics, ultrafast science, micro and nano fabrication, and optical information processing.

This rapid expansion has produced a rich yet fragmented landscape. Theoretical advances in wave topology, coherence theory, and vector multipole analysis develop in parallel with progress in laser and beam shaping technology, nanostructured components, and advanced detection schemes. Application driven work in communication [9, 11, 13–15], imaging [16], and materials processing [17–19] often exploits singular structures without always making the underlying topological framework explicit. Existing reviews and roadmaps on structured light have surveyed key aspects of this activity [5–8, 20], but a focused synthesis that places singularities and topology at the centre of the narrative across platforms and operating regimes has been missing.

To address this need, contributions are assembled from many of the researchers who have shaped singular optics and structured light. Each chapter combines a educational style exposition of current understanding with a forward looking assessment of outstanding challenges and emerging opportunities. Together they span fundamental theory, experimental techniques for generation and detection, and applications that range from precision metrology and imaging to communication, material manipulation, and nonlinear and quantum photonics. A particular aim is to expose common physical principles that recur in apparently different settings and to highlight conceptual and technological tools that are likely to guide future progress.

On the theoretical front, the chapters develop rigorous vector multipole descriptions of structured fields, explore coherence vortices and spatiotemporal optical vortices, and analyse the controlled evolution and motion of singularities for information processing and tailored beam propagation. Complementary contributions focus on mode characterization and detection, including optimal receiver strategies and sampled detection schemes for orbital angular momentum beams, deep learning assisted and speckle based structured light detection, and intensity autocorrelation based extraction of spatial modes, together with practical approaches for measuring topological charge, exploiting orbitalization ellipsometry, and using spin orbit conversion to retrieve nanoscale orientation and anisotropy. Application driven chapters address material manipulation with structured beams, high harmonic generation driven by vortex fields, coded aperture and random media imaging with topologically structured light, and high dimensional optical communication that leverages advanced spatial mode control. Taken together, the topics represented in this collection articulate the present capabilities of singular optics, reveal common physical principles that link seemingly disparate implementations, and identify key challenges whose resolution will enable robust singularity based technologies for next generation photonic systems.

2 A brief overview of singular optics (Carmelo Rosales-Guzmán and Valeria Rodríguez-Fajardo)

2.1 Generation and characterisation of optical singularities

The field of singular optics, encompassing singularities in the phase or polarisation of scalar or complex vector light beams, has become an active research field. This rapid development has been partly fuelled by pioneering applications in fields as diverse as optical manipulation, high-resolution microscopy, optical metrology, classical and quantum communications, among many others [4, 5, 21–23]. In parallel, researchers have invested considerable effort in developing a vast number of techniques for their generation, and more recently, in advancing characterisation methods and measures [5]. While generating phase singularities can be achieved in a relatively simple manner, for instance by using photographic printed holograms or spiral phase plates, generating polarisation singularities requires the simultaneous manipulation of two degrees of freedom, namely the spatial mode (the shape of light) and its polarisation state. To this end, several methods have been proposed, which can be classified into two main categories: manipulation of the geometric phase and manipulation of the dynamic phase. The former is based on the direct conversion of spin to orbital

angular momentum, achieved either through metamaterials or variable wave-plates (such as q-plates). The latter is commonly implemented through interferometric arrays or by controlling the spatial profile of both polarisation components. The advent of computer-controlled devices, specifically Liquid Crystal on Silicon Spatial Light Modulators (LCoS-SLMs) and digital micromirror devices (DMDs), completely reshaped the landscape of generation techniques for both phase and polarisation singularities, allowing unprecedented flexibility and versatility. Typical experimental setups for the generation of phase singularities using a SLM and polarisation singularities employing a DMD are illustrated in Fig. 1a and b, respectively. In the former, a linearly polarised light beam impinging on the screen of the SLM generates in the first diffraction order the desired phase singularity. In the latter, and given that DMDs are not sensitive to polarisation, two light beams with orthogonal polarisation impinge on the screen of a DMD, generating a vector beam in the first diffraction order.

Characterisation of optical singularities is of equal importance as generation methods. For instance, determining the topological charge associated with phase singularities is of relevance in various applications. Traditional methods employ the use of interferometric arrays, where the beam of interest is interfered with either a plane wave or with itself after inverting its phase (for example, with a Dove prism). Alternative methods analyse the far-field diffraction pattern produced when the beam interacts with an aperture. The use of refractive optical elements, which transform the azimuthal phase into linear phase gradients, commonly known as mode sorters, represents a more powerful technique. Contrary to phase singularities, the characterisation of polarisation singularities is still in its infancy, with Stokes polarimetry being the most popular choice as it provides a direct way to reconstruct the two-dimensional transverse polarisation distribution from intensity measurements. On the other hand, inspired by the mathematical similarity between polarisation singularities and quantum entangled states, the Vector Quality Factor (VQF) quantifies the entanglement or Concurrence (C) between the spatial and polarisation degrees of freedom. More precisely, the VQF assigns values in the interval [0, 1], zero to scalar beams and one to maximally entangled ones, and can be measured experimentally through projective measurements. When using SLMs, the unknown field is first split into its two polarisation components, each of which is projected onto six spatial filters encoded as digital holograms on the SLM. The on-axis intensity of the twelve combinations is measured in the far-field (typically, at the Fourier plane of a lens), from which the VQF is computed. If a DMD is used, the procedure is very similar, with the additional advantage that the number of required measurements can be reduced to a minimum of 8. The VQF can also be computed directly from the Stokes parameters in a basis-independent manner, avoiding the need for a priori knowledge of the spatial mode.

In what follows, a summary of some of the applications that have demonstrated the capabilities of both phase and

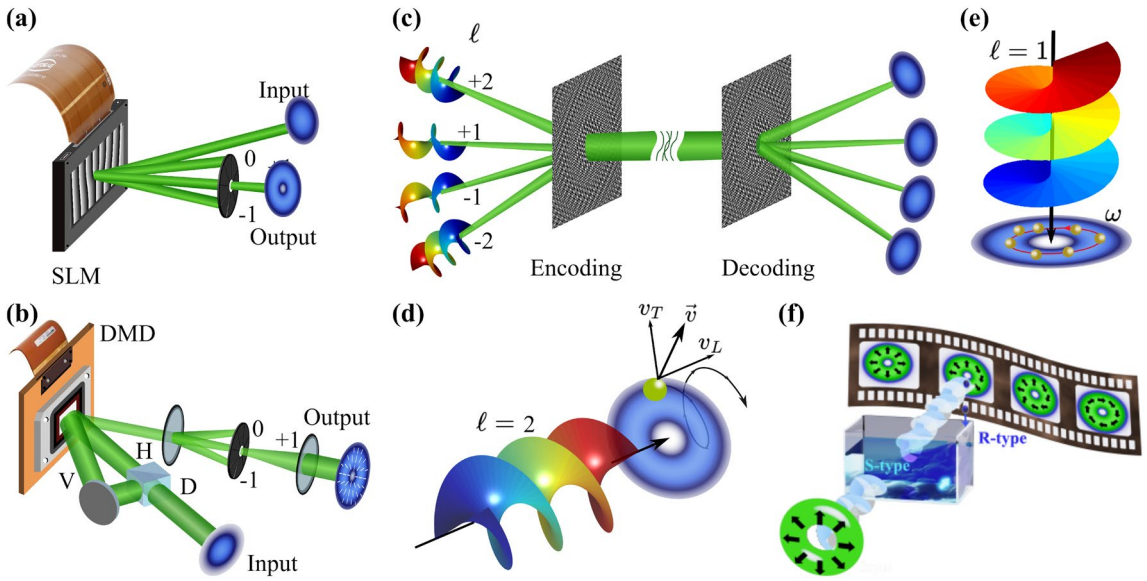

Fig. 1 **a** Schematic representation of the generation of phase singularities through a Spatial Light Modulator. **b** Typical experimental setup for generating polarisation singularities via a Digital Micromirror Device in a polarisation-insensitive technique. **c** Schematic representation of the use of optical vortices in a multiple input multiple output communications system. **d** Schematic representation of the use of phase singularities in laser remote sensing for measuring the full velocity vector. **e** Representation of the transfer of optical orbital angular momentum from optical vortices to microparticles. **f** Representation of the use of a vector beam in measuring the concentration of chiral molecules

polarisation optical singularities will be provided. While only those applications that from our perspective, have been particularly relevant will be covered, certainly many more will go unmentioned. For that, an apology in advance is given. That being said, here only applications in optical communications, optical metrology, optical manipulation, laser remote sensing and optical activity will be given.

2.2 Applications of optical singularities

For the past three to four decades, optical singularities have demonstrated their potential in a wide variety of applications in technological and scientific research fields. While these constitute an extensive set, only some distinct key application areas will be discussed here.

In the realm of Optical Communications, since current communication systems are approaching a fundamental limit in information transmission capacity, researchers are actively developing innovative techniques to overcome this. A possible solution relies on the use of orthogonal spatial modes with phase singularities, such as Laguerre-Gaussian modes, allowing for increasing the overall capacity in proportion to the number of spatial modes. Figure 1c illustrates schematically multiplexing and demultiplexing of spatial modes to transmit information. Similarly, beams with polarisation singularities have attracted considerable attention, in part due to their higher resistance to perturbations.

Laser remote sensing could also benefit from optical singularities, for example, in applications that require measuring the full velocity vector of moving objects. While the Doppler effect is commonly used to monitor speed, it only allows for determining the longitudinal velocity component, the one parallel to the beam's propagation direction. With this in mind, in 2011, Belmonte and Torres proposed a technique to measure the transverse velocity component using light beams with a transverse phase gradient, such as the ones in light beams with phase singularities. The key idea relies on the fact that such optical beams introduce energy flows in the direction perpendicular to their propagation. As such, the back-scattered light reflected from the moving target contains information about its position and velocity, which can be extracted from the Fourier transform of the intensity signal produced from the coherent interference of the backscattered light and a reference beam. Figure 1d shows a sketch of the simultaneous measurement of the longitudinal and transverse velocity components. Importantly, the same principle can be applied to measure the vorticity of fluids.

In the field of optical manipulation, although it was well-known since Kepler's time that light carries linear momentum, it was not until the beginning of the 18th century that it was predicted that light can also carry spin angular momentum associated with its circular polarisation. This was proved experimentally in 1936 by Beth [23], and later, in 1992, Allen and co-workers demonstrated that light beams with phase singularities also carry momentum, but in the form of orbital angular momentum. Soon after this, it was shown that this angular momentum can be transferred to microparticles, inducing rotations in a direction defined by the sign of the topological charge [4] (see Fig. 1e for a schematic illustration). Since then, this newfound ability to tailor the various properties of light has enhanced the capabilities of optical tweezers, where modification of the intensity, wavefront, and polarisation distributions allows the transport of microparticles along open and closed trajectories, establishing the basis for advanced optical manipulation techniques. For instance, light beams with polarisation singularities in combination with the photophoretic effect have been used for long-distance, stable, and switchable optical transport of microparticles.

Optical phenomena, such as optical rotation and circular dichroism, are particularly relevant in the food and drug industry, where the ability to differentiate between chiral molecules is crucial. These, also known as enantiomers, are pairs of molecules that are identical in most aspects except that they are mirror images of each other, making them difficult to differentiate. They become distinguishable, however, in their interaction with other chiral objects. While techniques capable of discriminating between enantiomers commonly rely on polarised light, in the last decade, it has been demonstrated that the orbital angular momentum of light can also engage with chiral molecules. Along this line, a vectorial version proposed recently, fully exploits the inhomogeneous polarisation distribution of vector beams [24] by monitoring the change in the polarisation distribution after traversing a chiral medium, thus enabling the position-dependent measurement of the concentration variations across different sample regions (Fig. 1f). This novel method paves the way for more complex schemes, such as the monitoring of chiral compound synthesis or the quantification of the concentration of organic compounds in the atmosphere.

At the quantum level, optical singularities have also gained popularity, particularly due to their potential to increase the security of quantum communication links. For instance, optical vortices allow the implementation of quantum key distribution (QKD) protocols in higher dimensions, thus increasing their security in proportion to the dimension of the encryption basis used. Furthermore, polarisation singularities, which benefit from the nonseparability between the spatial and polarisation degrees of freedom, are not only pioneering novel schemes for enhancing the security of quantum cryptography but also provide robust modes [25].

2.3 Conclusions and future perspectives

Here, a few key research fields where optical singularities have demonstrated real potential have been highlighted, as well as outlined a few techniques to generate and characterise light beams with such features. These are still in development, and many researchers are actively aiming to transfer them from the lab into the real world by making them faster, cost-effective or easier to implement.

There is no doubt, the full potential of optical singularities is still in a development stage. Certainly, as this manuscript is in preparation, researchers are working on novel applications, possibly pioneering unexplored research fields. The goal is to advance or even unveil applications, especially ones that have been challenging with conventional approaches, but become feasible with engineered optical fields, such as optical singularities. Along the same line, the proposal of generation techniques with high refresh rates, which have become possible thanks to DMDs, is paving the path for novel approaches that require the use of dynamic input fields, such as in real-time optical metrology. Similarly, the implementation of innovative characterisation techniques is of great relevance in various research fields and will undoubtedly positively impact their capabilities. Importantly, the introduction of Artificial Intelligence (AI) will be decisive in advancing all areas of the field. For instance, conventional techniques for detecting optical singularities are being replaced by methods based on neural networks, a research direction that is evolving very rapidly. In a similar way, a research line that is gaining popularity very fast involves the study of optical singularities with higher resilience to disturbances, for example, upon propagation in turbulent free space. Finally, it is necesary to emphasise that, although the field of singular optics has progressed considerably since its beginnings, it will continue evolving in multiple directions, gaining traction in traditional and new applications and fields, where light's fascinating properties are improving current approaches as well as inspiring innovative ones.

3 Vector multipoles: a rigorous and efficient framework for singular optics (Matthew R. Foreman)

3.1 Background

Optical beams possessing singular phase and polarisation structures have become an important vehicle for focus shaping, with applications ranging from laser trapping and particle manipulation to super-resolution microscopy and lithography. Prominent among such structured beams is the family of cylindrical vector vortex (CVV) beams, which carry orbital angular momentum (OAM) and can produce narrow or ring shaped focal distributions used in e.g., stimulated-emission-depletion (STED) microscopy or minimal fluorescence photon flux microscopy (MINFLUX) [4, 6].

Utility of singular beams is often realised upon focusing by high numerical aperture (NA) optics. A rigorous understanding of the resulting field distributions in the focal region is therefore essential. The gold-standard tool for such analysis is the Debye-Wolf vectorial diffraction integral [26], which although highly accurate can be computationally intensive and offers limited physical insight. In this chapter we report on a complementary approach which represents the focused field as a superposition of vector multipoles, thereby not only providing an efficient computational framework whilst maintaining physical rigour, but also enabling deeper understanding of CVV beams, their focal properties and their interactions with matter.

3.2 Methodology

The foundation of our methodology is to represent the angular spectrum of an arbitrary focused CVV beam in a basis of vector multipoles, thereby establishing a direct link between the user-defined field in the pupil of a high NA lens and the electromagnetic modes that constitute the resulting focussed field [27]. A general CVV beam can be described in the exit pupil of a focusing lens by the generalised Jones vector

$$\begin{bmatrix} \widetilde{E}_x^{\mathrm{col}}(\theta,\phi) \\ \widetilde{E}_y^{\mathrm{col}}(\theta,\phi) \end{bmatrix} = \begin{bmatrix} \cos(p\phi+\phi_0) \\ \sin(p\phi+\phi_0) \end{bmatrix} \widetilde{E}(\theta) e^{in\phi} \tag{1}$$

where $(\sin\theta,\phi)$ define the polar coordinates of positions in the pupil, $\widetilde{E}(\theta)$ describes the radial amplitude variation across the beam, n and p ($\in \mathbb{Z}$) are the topological charge and cylindrical vector order respectively, and ϕ_0 is a constant (see Fig. 2a for a taxonomy of common CVV beams). Assuming the lens is telecentric, vectorial ray tracing can be used to transform Eq. (1) onto the Gaussian reference sphere where it can be expressed (in spherical polar components) as [26]

$$\begin{bmatrix} \widetilde{E}_\theta(\theta,\phi) \\ \widetilde{E}_\phi(\theta,\phi) \end{bmatrix} = a(\theta)\widetilde{E}(\theta) \begin{bmatrix} e^{i\Phi_-} + e^{i\Phi_+} \\ ie^{i\Phi_-} - ie^{i\Phi_+} \end{bmatrix} \tag{2}$$

where $\Phi_\pm = m_\pm\phi \pm \phi_0$, $m_\pm = n \pm p \mp 1$ and $a(\theta)$ is an apodisation factor that incorporates the finite NA of the system. Equation (2) represents the angular spectrum of the beam that will be brought to a focus [26]. The focused electric field can however be represented as a superposition of vector multipoles, i.e., in the form $\mathbf{E}(\mathbf{r}) = \sum_\nu \sum_{l,m} a_{lm}^\nu \mathbf{E}_{lm}^\nu(\mathbf{r})$, where a_{lm}^ν are the weighting coefficients for electric ($\nu = E$)

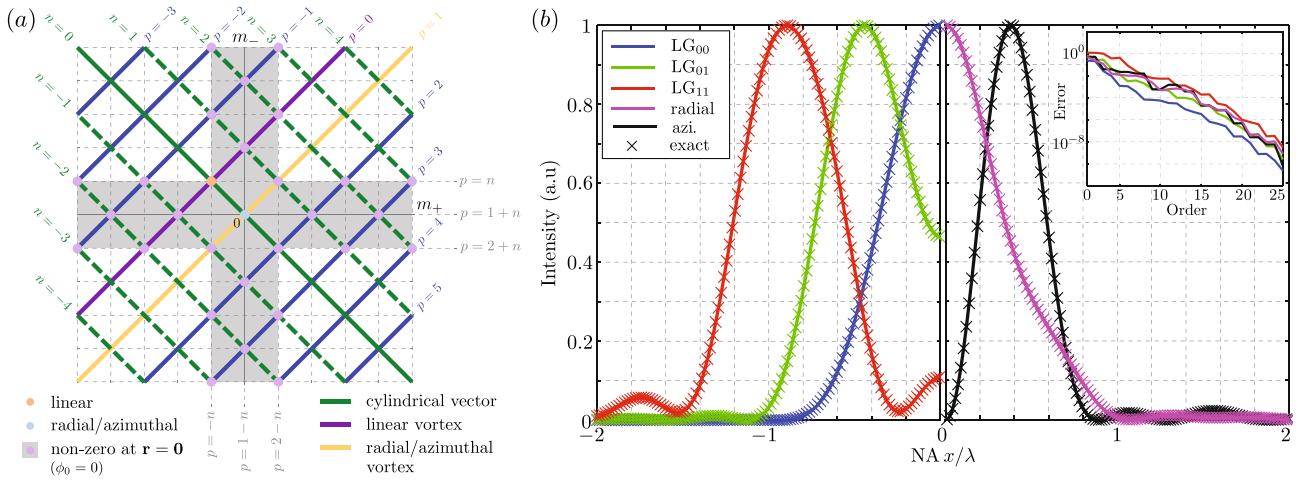

Fig. 2 **a** Taxonomy of some CVV beams defined by orders n and p (equivalently m_+ and m_-). **b** Normalised intensity linescans along the x-axis for focused LG vortex, radially and azimuthally polarised vector beams (symmetric about $x = 0$) as calculated using the multipole method. (Inset) Integrated relative RMS error between multipole representation and exact result found using the Debye-Wolf integral for differing truncation l orders

and magnetic ($\nu = M$) multipoles of order (l, m). Since the focused field must be finite at the origin, the multipole fields $\mathbf{E}^{\nu}_{lm}(\mathbf{r})$ are constructed using spherical Bessel functions of the first kind. Matching the far field forms of the multipoles to the beam's angular spectrum (Eq. (2)) yields integral transforms that directly link the pupil field to a^{ν}_{lm} and hence $\mathbf{E}(\mathbf{r})$. Two distinct cases arise depending on the CVV beam parameters. For the general case where $m_+ \neq m_-$ (i.e., $p \neq 1$), the symmetries of the problem leads to $a^{\nu}_{lm} = 0$ for $m \neq m_{\pm}$ and $a^{E}_{l,m_{\pm}} \propto \mp a^{M}_{l,m_{\pm}}$, where

$$a^{E}_{l,m_{\pm}} = A_{l,m_{\pm}} e^{\pm i\phi_0} \int_0^{\alpha} a(\theta)\widetilde{E}(\theta)\Theta^{\mp}_{l,m_{\pm}}(\theta)\sin\theta d\theta, \tag{3}$$

α is the semi-angle of convergence of the lens, A_{lm} is a mode dependent constant and $\Theta^{\pm}_{l,m}(\theta)$ are functions involving derivatives of the associated Legendre polynomials [28]. A similar, albeit more involved one-dimensional (1D) integral can also be found for the $m_+ = m_-$ case (e.g. radial or azimuthal polarisations) [28].

3.3 Results

The multipole decomposition described reduces the Debye-Wolf integral to a discrete spectrum of multipole modes, whose coefficients are given by simple 1D integrals. In so doing, the formalism provides an efficient and accurate method to calculate the focal distribution of a CVV beam (Fig. 2b). Evaluation of a full focal distribution can, for example be achieved in a few seconds (or less) on modern day computers. Moreover, the multipole approach provides a powerful lens through which to analyse fundamental properties of focused singular beams and their applications in light-matter interactions, as we now discuss.

Focal structure: A primary question in focus shaping is whether a beam will produce a bright spot or a dark "hole" at the geometric focus ($\mathbf{r} = \mathbf{0}$). The multipole framework provides a clear answer, since only electric dipole modes ($\nu = E, l = 1$) possess a non-zero electric field at $\mathbf{r} = \mathbf{0}$. Therefore, a necessary condition for obtaining a bright focal spot is that the CVV beam contains electric dipole contributions in its multipole spectrum (equivalently $|m_{\pm}| \leq 1$). High-order CVV beams violating this condition will produce a null field on-axis. It must be noted that a non-zero on-axis energy density is however not sufficient to ensure a spot-like focus, as strong side lobes from higher-order multipoles may dominate. The family of multipolar beams, i.e. those containing only a single non-zero multipole coefficient, provide a convenient class of CVV beams for which focal properties follow without such complications. Nevertheless, the multipole representation allows for rapid calculation of the full focus to verify the structure in all cases.

Angular momentum: The angular momentum (AM) content of a focused CVV beam can be understood through its constituent multipoles. For example, we can analyse the spin (SAM) and orbital (OAM) components of the AM flux of pure multipolar CVV beams [29]. A key result is that for a (l, m) multipole beam, the ratio of the total integrated axial AM flux to the total energy flux is conserved upon propagation, focusing or imaging, and is equal to m/ω. The relative contributions of SAM and OAM to the total flux in a focusing geometry, however, depend strongly on the NA of the focusing lens. For a single multipole beam, as NA increases, there is a distinct conversion of SAM flux into OAM flux (spin-orbit exchange SOE). The strength of SOE depends

on the multipole order, with SOE becoming more significant at lower NAs for higher l, or conversely relative SAM flux reduces for higher m at higher NA. By choice of input beam structure and focusing NA, one can hence control the balance of SAM and OAM in the focal volume, so as to e.g. induce different types of rotation and torque in particle manipulation tasks.

Enhanced light–matter interactions: Interaction of focused singular beams with metallic nanoparticles (NPs) is central to many applications in enhanced spectroscopy, biosensing, and nanoscopy. The multipole representation is particularly advantageous here, as scattering of light by spherical NPs can be solved analytically using Mie theory. By combining these approaches it can be shown that the plasmonic field enhancement at the centre of a multi-layer spherical NP is independent of the illumination beam if it contains an electric dipole component [26]. Structuring of the illumination beam, however, becomes critically important when considering field enhancements away from the NP centre, particularly in the near-field region close to its surface. Average enhancement factors over the NP surface are ultimately dictated by the multipole content of the focused beam. For instance, focused LG_{00} and radially polarised beams are both dominated by electric dipole contributions, and thus produce similar effective enhancements, whilst in contrast, a focused azimuthally polarised beam is instead dominated by magnetic dipoles, leading to distinct behaviour. Knowledge of the dominant multipole components of a focussed CVV beam can thus direct NP design to ensure efficient excitation of specific plasmonic modes and achieve optimal near field surface enhancements [26].

3.4 Conclusions and future perspectives

By transforming the challenge of modelling intricate vectorial fields into the more tractable problem of analysing a discrete spectrum of multipole components, the multipole expansion offers a rigorous, efficient, and physically intuitive framework to describe tightly focused singular beams. Indeed, we have discussed how the multipole approach can provide powerful insights into complex properties of CVV beams, such as their focal structure, angular momentum content and interactions with plasmonic nanoparticles. Looking forward, this methodology can greatly simplify analytical modelling and numerical calculations, making inverse-design and optimisation of light– matter interactions with singular beams more accessible. Moreover, in imaging applications, such as localisation microscopy, the fitting of computationally intensive point spread functions is a major bottleneck. The speed and accuracy of the multipole approach, achieved by exploiting the analytic symmetries of the problem and its implementation via efficient 1D integrals, makes it highly amenable to modern parallel processing on CPUs and GPUs. This could therefore significantly accelerate the analysis of large datasets, paving the way for high-throughput applications in the future.

4 Coherence vortices: generation and detection (Amit Yadav, Sarita, Akanksha Gautam,and Rakesh Kumar Singh)

4.1 Background

Vortex beams (VBs) are a fascinating class of light beams, characterized by their helical phase structure with azimuthal angle dependence $\exp(il\phi)$, where l is the topological charge (TC) of the vortex beam and ϕ is the azimuthal angle. Several techniques have been developed to generate coherent vortex beams, including computer generated holograms, q plates, mode converters, and many more. Recently, research on vortex beams has been extended from fully coherent to partially coherent vortex beams (PCVBs) for several reasons. As a PCVB propagates, the phase singularities gradually diminish. Nevertheless, PCVBs can still manifest hidden singularities, which originate from the two point correlation function and are known as coherence vortices (CVs). The presence of coherence vortices (CVs) as ring shaped dislocations in the cross correlation function was first identified by Palacios et al [30].

Several methods have been employed to generate and detect the CVs, including using three equally spaced circular apertures at the source plane to create a coherence vortex array [31]. Akanksha et al. proposed a technique to induce a helical phase structure in the two-point correlation function by employing the polarization basis of light. Recently, Yadav et al. proposed a method of detecting the phase singularities in the low coherence background [32], Xingyuan Lu et al. gave an idea of phase detection of coherence singularities by introducing a movable perturbation at a certain point in an illumination window, Zhu et al. developed a scheme for cross-spectral density phase measurement with an off-axis reference point to measure coherence singularity distribution of PCVB. Therefore, given the significant advantages of CVs, their generation and detection hold crucial importance. Here, we discuss the role of the van Cittert-Zernike theorem in shaping complex coherence and one of our recently developed methods for generating coherence vortices using a binary pinhole mask [33]. The Van Cittert–Zernike theorem connects an incoherent source and its two-point correlation function in the far-field, stating that the two-point correlation function is the Fourier transform of the source's intensity distribution [34].

4.2 Methodology

Figure 3a and b represent different classes of vortices and a scheme for tailoring the complex coherence of light using a suitable mask. The mask is made up of a total number N of pinholes. The radius $v(n)$ and azimuthal angle $\theta(n)$ of the n th pinhole from the center are set over the transverse plane such that

$$v(n) = \left(\frac{lz\lambda\,\theta(n)}{\pi} + v_0^2\right)^{1/2}, \tag{4}$$

where,

$$\theta(n) = \frac{2\pi n}{N}, \tag{5}$$

where v_0 is the initial radius from the center to the first pinhole, l is the TC, λ is the wavelength, and z is the distance from the pinhole mask to the observation plane. To measure the complex coherence properties of the generated beam from the binary pinhole mask, a Sagnac shearing interferometer was employed. Using the four step phase shifting technique, the recorded intensity at the detector plane was expressed as

$$I(\theta) \approx I(\mathbf{r}_1) + I(\mathbf{r}_2) + 2\sqrt{I(\mathbf{r}_1)I(\mathbf{r}_2)}\, g(\Delta\mathbf{r}) \cos\left[\phi(\Delta\mathbf{r}) + 2\theta\right], \tag{6}$$

where $I(\theta)$ is the intensity and $I(\mathbf{r}_1)$ and $I(\mathbf{r}_2)$ are the intensities at points $\mathbf{r}_1$ and $\mathbf{r}_2$. The term $g(\Delta\mathbf{r})$ represents the fringe visibility and 2θ is the introduced phase shift. The four phase shifting algorithm is subsequently applied to retrieve the fringe visibility and the corresponding phase as

$$g(\Delta\mathbf{r}) \propto \frac{\sqrt{\left[I(0) - I(\pi)\right]^2 + \left[I(\frac{\pi}{2}) - I(\frac{3\pi}{2})\right]^2}}{I(0) + I(\frac{\pi}{2}) + I(\pi) + I(\frac{3\pi}{2})}, \tag{7}$$

$$\phi(\Delta\boldsymbol{r}) = tan^{-1}\left[\frac{I(\frac{3\pi}{2}) - I(\frac{\pi}{2})}{I(\pi) - I(0)}\right]. \tag{8}$$

Here, $g(\Delta r)$ and $\phi(\Delta r)$ are the amplitude and phase of the complex spatial coherence function and are represented as $W(\Delta r) = g(\Delta r)\exp[i\phi(\Delta r)]$. To further confirm the formation of CVs, the complex coherence function is analyzed using the orthogonal projection method. These vortices appear in the two point correlation function and differ from the phase singularities in the complex fields. Some commonly discussed vortices in optics are shown in Fig. 3a.

4.3 Results

Figure 3b presents the schematic for tailoring the two-point correlation function using the van Cittert Zernike theorem and an experimental technique to measure the complex spatial coherence function. Figure 3c illustrate the reconstructed amplitude and phase distributions of the complex coherence function produced by the binary pinhole mask. The magnitude of the complex coherence function exhibits a doughnut-shaped profile in the amplitude, while the phase map reveals a helical phase structure, confirming the generation of a CVs. Furthermore, Fig. 3d shows the modal decomposition of the coherence vortex spectrum, which verifies the TC of the coherence vortices.

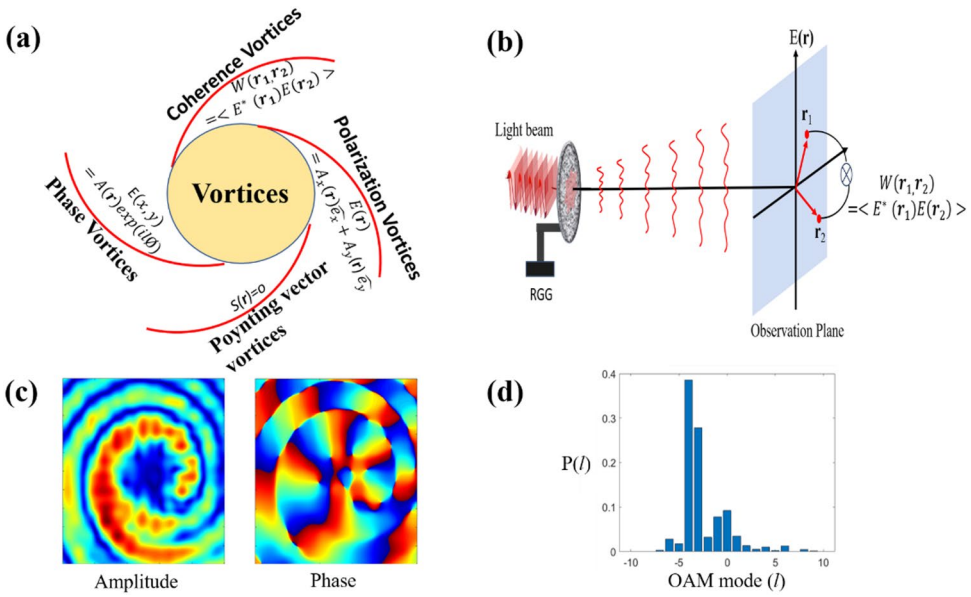

Fig. 3 The figure shows **a** different types of vortices, **b** the schematic for recording the two-point correlation function, **c** the amplitude and phase of the CVs with helical phase structure, **d** the modal decomposition of CVs. RGG: rotating ground glass

4.4 Conclusions and future perspectives

In conclusion, we discussed the trends in the generation and detection of coherence vortices and presented a method for their generation and detection. Here, vortices are generated in a two-point complex correlation function in contrast to conventional vortices in the complex optical field.

5 Deterministic vortices in partially coherent beams (Greg Gbur)

5.1 Background

Vortex beams have been considered for a wide variety of applications, most notably free– space optical communication, but atmospheric effects inevitably distort or remove singularities from a wavefield on propagation. It has been demonstrated that partially coherent beams tend to be more robust to atmospheric distortion, which has led to an interest in combining partial coherence and vortex structures. However, as discussed in Sect. 4, partial coherence and vortices typically do not "play nice" together: a vortex is a phase structure of a field, while a partially coherent field by definition has a randomly fluctuating phase. Singularities imparted on a partially coherent field will typically evolve into singularities of the two-point correlation function, which indicates that they are no longer a definite and deterministic part of the wavefield.

It has now been demonstrated, however, that there are a number of distinct ways to impart a deterministic or nearly deterministic vortex on a partially coherent beam. The beam classes that arise from these approaches may provide a more reliable way to transmit topological structures over long propagation distances. Here we review a number of these approaches.

5.2 Methodology

The cross-spectral density of a beam of light at frequency ω may always be written in the factorized form,

$$W(\mathbf{r}_1, \mathbf{r}_2, \omega) = U^*(\mathbf{r}_1) U(\mathbf{r}_2) \mu(\mathbf{r}_1, \mathbf{r}_2), \tag{9}$$

where $\mathbf{r}_1$ and $\mathbf{r}_2$ are the position vectors of two spatial points, $U(\mathbf{r})$ represents a monochromatic field and $\mu(\mathbf{r}_1, \mathbf{r}_2)$ represents the spectral degree of coherence. We refer to a field as possessing a *deterministic vortex* (DV) if there is a vortex phase structure present in the field $U(\mathbf{r})$; a typical coherence vortex will arise in the spectral degree of coherence.

The earliest example of a DV in a partially coherent field was introduced in 2001 by Ponomarenko [35], who showed that it is possible to create a mathematical class of beams with a closed form expression with a separable azimuthal phase, i.e.

$$W(\mathbf{r}_1, \mathbf{r}_2, \omega) = w(\rho_1, \rho_2) e^{im(\phi_2 - \phi_1)}, \tag{10}$$

where m is the vortex order and (ρ, ϕ) represent the transverse coordinates of the beam in polar form. These beams have a definite vortex phase structure that persists on propagation in free– space and is associated with a zero of intensity on axis. More recently, Mei et al. [36] demonstrated that it is possible to construct a very general class of vortex beams that not only possess a persistent on-axis DV but can be designed to self-focus as a desired propagation distance. Beams of separable phase form have been shown to be resistant to turbulence-induced distortion.

It is also possible to have beams that manifest a DV in the far zone, even though they only possess coherence vortices at any intermediate propagation distance. In 2020, Zhang, Cai and Gbur constructed [37] an entire class of such partially coherent vortex beams using a beam wander model for a partially coherent field of the form,

$$W(\mathbf{r}_1, \mathbf{r}_1, z; \omega) = \int P(\mathbf{r}_0)\, U_m^*(\mathbf{r}_1 - \mathbf{r}_0, z)\, U_m(\mathbf{r}_2 - \mathbf{r}_0, z)\, \mathrm{d}^2 r_0, \tag{11}$$

where $U_m(\mathbf{r}, z)$ represents a coherent vortex beam of order m with its axis shifted by $\mathbf{r}_0$ and $P(\mathbf{r}_0)$ represents the probability density for the beam axis to appear at $\mathbf{r}_0$. Because an axis shift is converted to a beam tilt in a Fourier transform operation like far zone propagation, the far zone consists of a collection of superimposed vortex beams with the same central axis and distinct tilt phases, resulting in an on-axis vortex.

Building on this observation, Miao, Zhang and Gbur demonstrated [38] that a DV can be placed at an arbitrary propagation distance by using a fractional Fourier transform in the design process. The field in this case can have any degree of coherence and still produce a deterministic vortex at the designed distance, though the depth of field for this vortex decreases as the spatial coherence is decreased.

Through the use of Bessel beams, it is even possible to make a DV that revives periodically on propagation, as shown by Qi and Gbur [39]. In the simplest incarnation, the beam consists of two modes, namely a vortex mode $U_m(\mathbf{r})$ of order m incoherently combined with a coherent superposition of zeroth-order Bessel beams in such a way to produce a periodic zero on axis. These beams are combined as

$$W(\mathbf{r}_1, \mathbf{r}_2, \omega) = U_m^*(\mathbf{r}_1) U_m(\mathbf{r}_2) + U_0^*(\mathbf{r}_1) U_0(\mathbf{r}_2). \tag{12}$$

At those positions where $U_0(\mathbf{r})$ vanishes on axis, the vortex mode will dominate and the beam will become very close to a perfect DV.

5.3 Results

We illustrate one example of a deterministic vortex revival in Fig. 4. The second-order on axis vortex decomposes into two first-order coherence vortices, and the zero ring of the Bessel beam decomposes into two negative first-order vortices. At $z = 50$ m , however, the second-order vortex reconstitutes. In this case, the vortex is not a perfect DV, but it is very close to one and could be said to be strongly bound to the low intensity spot on-axis.

5.4 Conclusions and future perspectives

The examples presented here show that there are many ways to construct deterministic vortex beams, including possibilities not yet explored. These beams have the potential to produce a stable on-axis vortex at a desired propagation distance (or distances), which suggests that they could be good candidates for information carriers in free– space optical communication, taking advantage of both the robustness of partial coherence and the stability of coherent vortices.

6 Spatio–temporal optical vortices (Judy Kupferman and Shlomi Arnon)

6.1 Introduction and motivation

spatio–temporal optical vortices (STOVs) are a class of structured ultrafast light fields that couple spatial and temporal degrees of freedom in a nonseparable way. Their electric field phase winds helically in a mixed space–time (x, t) or space– frequency (x, ω) plane, producing a phase singularity where the amplitude vanishes and the phase circulates by integer multiples of 2π. Unlike conventional vortices whose orbital angular momentum (OAM) is aligned with the propagation axis, STOVs carry transverse OAM oriented perpendicular to propagation. This additional degree of freedom enables light–matter interactions and information channels that are inaccessible to traditional spatial or temporal vortices. Ultrashort pulse lasers are essential for their creation, since their broad spectral bandwidth and temporal coherence permit simultaneous spatial and temporal phase control. Coherent manipulation of frequency components produces localized temporal phase singularities and space–time helical wavefronts with sub picosecond structure. Such control enables STOVs to mediate nonlinear interactions, probe ultrafast material responses, and encode information in high dimensional bases for classical and quantum

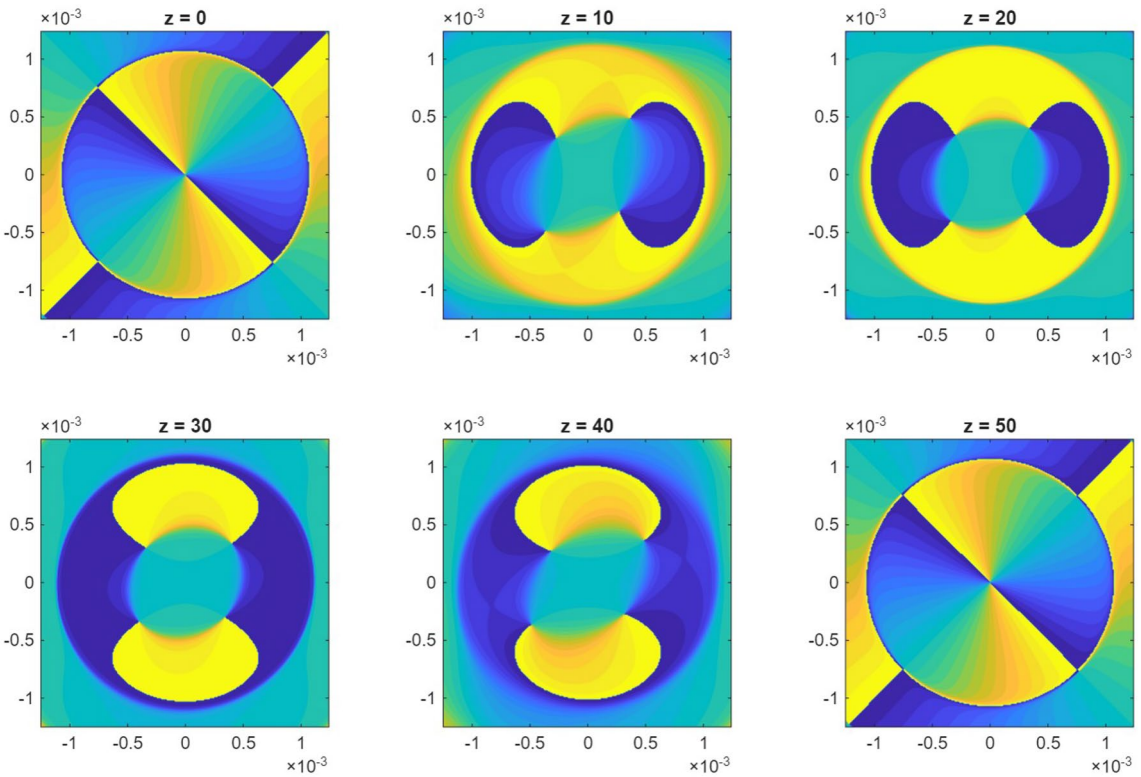

Fig. 4 Evolution of a deterministic vortex revival in a Bessel beam, designed to revive at $z = 50$ m. The wavelength is 500 nm, the lobe of the fundamental Bessel beam component is 0.5 mm, and the vortex order is $m = 2$

communication [40, 41]. From a fundamental perspective, their hybrid phase structure challenges conventional separations between spatial and temporal modes, motivating studies of optical topology beyond the paraxial regime, including topological charge conservation, time–frequency entanglement, and unconventional OAM exchange in ultrafast systems.

6.2 Theory and concepts

STOVs can be viewed as wave packets whose complex phase exhibits a singularity in a transverse spatial coordinate x versus time t or frequency ω. The topological charge l defines the number of 2π phase windings around this singularity, and the resulting transverse OAM enables angular momentum transfer orthogonal to propagation, which is distinct from conventional longitudinal OAM. Mathematically, STOVs are synthesized by applying a frequency dependent helical phase to a spectrally dispersed ultrafast pulse and recombining it in time. A chirped pulse dispersed along x and imprinted with a phase factor $\exp[il\Phi(\omega)]$ forms a vortex in the (x,t) plane after an inverse Fourier transformation. Propagation through dispersive or nonlinear media can distort this structure through self phase modulation or dispersion, which requires coupled spatio–temporal simulations of the nonlinear Schrödinger equation and Fourier optics [42]. The transverse OAM carried by STOVs also drives unique light–matter interactions: inducing torque on microscopic particles, mediating frequency conversion with new angular-momentum conservation rules, and shaping energy–momentum transfer in nonlinear processes. These effects underpin emerging applications in ultrafast spectroscopy, micromanipulation, and optical communication.

6.3 Experimental generation

STOVs are typically produced using femtosecond Ti sapphire or Yb based lasers. A standard setup employs a 4f pulse shaper in which two gratings and lenses spatially disperse the pulse spectrum, while a spatial light modulator (SLM) or phase mask at the Fourier plane imposes a helical, frequency dependent phase. Upon recombination, the beam acquires a helical phase in both space and time. Diagnostics such as frequency resolved optical gating (FROG) and spatially resolved spectral interferometry (SRSI) reveal the vortex structure and its temporal evolution. Several complementary generation approaches have emerged. (1) Four f pulse shapers and holography use SLMs or etched masks to impose helical spectral phases, which allows reconfigurable topological charge and real time tuning [40]. Although alignment sensitive, these methods remain highly flexible. (2) Metasurfaces and diffractive elements use nanostructured subwavelength features to imprint STOV phases directly, providing compact, lithographically reproducible sources [43]. The main challenges here include control of dispersion across broad bandwidths. (3) Nonlinear generation exploits second harmonic, sum frequency, or parametric processes to create or transfer transverse OAM between interacting waves, thereby accessing new spectral regions [44]. (4) Fiber and integrated photonics harness engineered modal dispersion in multimode fibers or on chip waveguides to generate STOV like states [42, 44]. These methods promise scalable and robust on chip sources but must mitigate dispersion induced distortions. Across all methods, ultrafast lasers remain indispensable, since they provide both the bandwidth required to localize singularities and the peak power needed for nonlinear coupling that underpins vortex formation.

6.4 Numerical modelling and simulation

Numerical methods are indispensable for understanding and optimizing STOVs, whose spatio– temporal coupling demands full-field simulations incorporating diffraction, dispersion, and nonlinear effects. The split-step Fourier method efficiently solves the NLSE, capturing the interplay between dispersion and Kerr nonlinearity, while beam propagation methods (BPM) are widely used for guided systems, accounting for modal dispersion and confinement in fibers or integrated platforms. Fourier optics simulations replicate experimental generation systems such as 4f shapers or metasurfaces to design phase masks that yield the desired vortex topology. Topological analysis complements these methods by tracking singularities, points where optical phase is undefined, revealing vortex creation, annihilation, and charge inversion during propagation, as well as stability and conservation laws governing transverse OAM. Together, these computational tools bridge theory and experiment, enabling predictive design and deeper understanding of spatio– temporal topology in structured light.

6.5 Challenges and future perspectives

Despite rapid progress, several challenges remain. Broadband, low-loss generation across femtosecond bandwidths requires achromatic metasurfaces and dispersion-engineered devices with high efficiency. Characterization remains difficult since STOVs exist in hybrid space– time domains, demanding sub-picosecond temporal and sub-micron spatial precision in interferometric imaging. For communication applications, scalable multiplexing of multiple orthogonal STOV channels requires phase-stable generation and minimal crosstalk, while propagation stability through nonlinear or dispersive media demands adaptive phase correction or

dispersion-compensated environments to preserve vortex integrity. Continued convergence of ultrafast laser science, computational photonics, and nanofabrication promises to expand STOV capabilities. As modeling and diagnostics advance, the ability to engineer light's full spatio–temporal topology will transform both fundamental and applied optics. STOVs are poised to become a cornerstone of future photonics, linking singularity physics, integrated devices, and structured information carriers in next-generation ultrafast systems.

7 Singularities in motion: topological evolution for information processing (Ahmed H. Dorrah)

7.1 Background

Among the many ways light can carry structure, optical vortices stand out by encoding orbital angular momentum (OAM) in the helical winding of phase around singularities. While the total charge is conserved as the beam propagates, the singularities themselves are not fixed. They shift, divide, coalesce, or vanish without perturbing the global charge. This delicate balance captures the essence of singular optics. For instance, it is well established that superpositions of OAM states can produce discrete jumps in effective charge along the optical path [45]. Likewise, spiral apertures can impose a linear chirp on the vortices' OAM, while temporal analogues such as self torque pulses with time dependent charge have extended the concept beyond spatial modes [46].

This raises a key question: can charge evolution go beyond discrete steps or linear chirps to form a deterministic, continuous progression that can be designed and used for complex tasks?

7.2 Methodology: rotatum of light

Rotatum of light represents a new class of vortex beams whose topological charge evolves in a continuous and deterministic manner along the propagation axis, providing a canonical realization of charge evolution [47]. These beams exhibit a quadratic variation of effective charge with propagation, which arises from the logarithmic-spiral migration of peripheral singularities toward the beam core. Such ordered migration produces a self-similar pool of singularities following scaling patterns reminiscent of phyllotaxis, seashell growth, and Fibonacci sequences as depicted in Fig. 5a. Rotatum beams therefore reveal that optical singularities can self-organize according to universal geometric rules, much as Bénard or Turing patterns reveal pattern-forming instabilities in matter. Here the instability is topological, encoded in the steady inward displacement of phase defects.

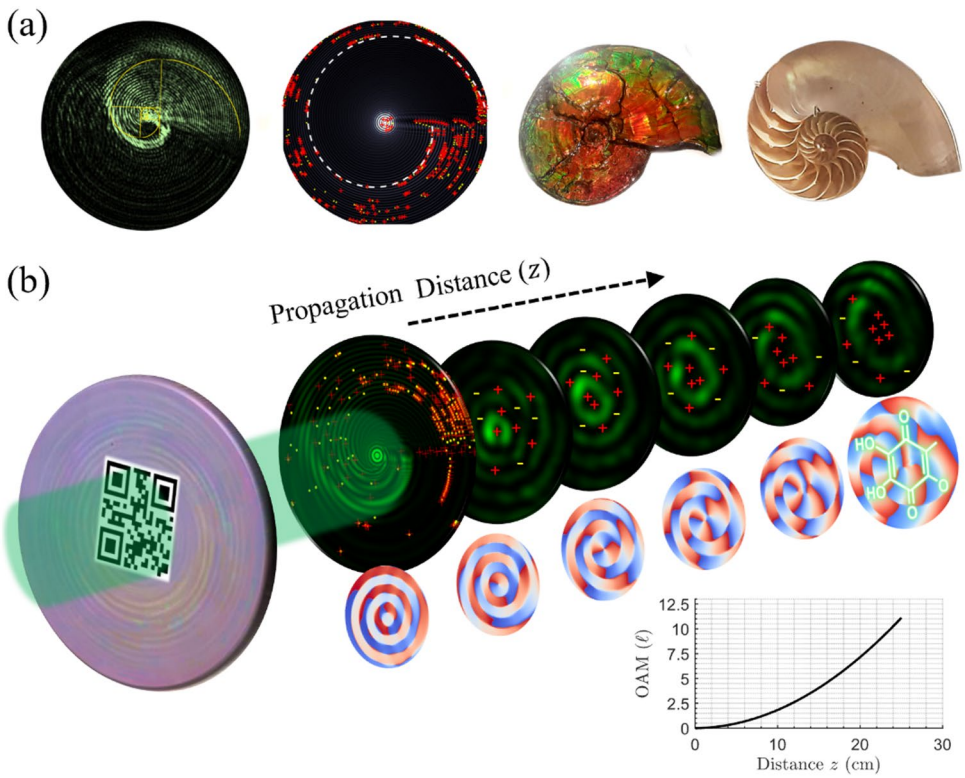

Fig. 5 Singularities in motion for information processing. **a** Vortex beam with optical rotatum showing phase singularities arranged along a logarithmic spiral, alongside natural analogues in an aragonite crystal and a nautilus shell. **b** Intensity and phase profiles of a vortex beam whose orbital angular momentum increases quadratically along propagation, with red and yellow markers denoting singularities of opposite helicity. The same optical framework is extended to reservoir computing, where structured optical fields perform complex information-processing tasks such as mapping encoded inputs to functional outputs

Notably, such adiabatic evolution introduces an additional Berry (Gouy) phase which causes a shift in the effective propagation constant and leads to measurable changes in beam size and spatial frequency. Rotatum beams thus link continuous topological evolution directly to controllable wave dispersion. Optical vortices of this kind can be experimentally generated using holographic masks, realized via spatial light modulators (SLMs). Alternatively, metasurfaces offer a more compact and robust platform that can sculpt spatial frequency content with subwavelength precision, while effectively harnessing spin and orbital momentum degrees-of-freedom using shape birefringence [48].

7.3 Results

The pool of singularities in a rotatum beam behaves as a deterministic dynamical system, meaning that for a fixed input field and phase mask the axial evolution repeats within measurement error. At each propagation distance z, the system state is set by the locations and charges of the singularities, and the effective charge $l(z)$ follows a smooth quadratic trajectory as shown in Fig. 5b. This repeatability yields stability and straightforward calibration, while the controlled growth of the lattice supplies a rich variety of field patterns. Accordingly, sampling the beam at multiple axial planes expands the input into a high dimensional set of features that retain memory of earlier planes. This mirrors the paradigm of reservoir computing [49], where the rotatum lattice acts as a fixed, complex reservoir that nonlinearly transforms and temporally embeds the input. Consequently, a trained, simple readout (for example, linear) combines those features to perform the chosen task, such as classifying input patterns, estimating continuous parameters (aberrations, channel state, bioactivity of a molecule), or short horizon prediction, without reconfiguring the optical medium itself.

In contrast to scattering based reservoirs, rotatum lattices offer tunability and reproducibility. The curvature $\mathrm{d}^2\ell/\mathrm{d}z^2$ controls the strength of the nonlinear input output mapping, while the diffraction length z_R and the sampling interval Δz set the effective memory depth. The spiral arrangement of singularities is approximately self similar, which adds redundancy and robustness to noise and fabrication tolerances. With axial readout, rotatum beams have the potential to enable a paradigm for volumetric optical processors in which computation is naturally distributed along the propagation axis.

Extending beyond a single beam, arrays of rotatum beams can introduce controlled coupling through diffraction, interference, or even cavity feedback, enabling collective states such as synchronization and defect nucleation across multiple rotatum threads. Such controlled coupling, possibly realized using large metasurface arrays, maps naturally to graph-based computation, while multi-beam interference scales the reservoir by adding memory and effective dimensionality to the ensemble.

7.4 Conclusions and future perspectives

Continuous topological evolution offers new opportunities across several domains beyond computing. In communications, a rotatum beam generates a sequence of effective charges along the propagation axis expanding beyond conventional vortex beams which carry a fixed OAM state. Therefore, receivers at different planes can detect distinct states without lateral demultiplexing. In micromanipulation, the quadratic chirp of rotatum transforms constant torque into a tunable waveform, allowing trapped particles to be accelerated, decelerated, or driven in oscillation—extending optical tweezers into new regimes. In materials processing, the spiral lattice of singularities provides a template for volumetric structuring in photoresponsive media, offering a route to encode growth-like geometries into matter. In quantum optics, pumping a nonlinear medium with rotata yields a deterministic trajectory of OAM states. This allows the resulting photon correlations to evolve with distance, enlarging the accessible Hilbert space and supporting hybrid time–space– OAM protocols with continuously modulated entanglement.

Beyond single-beam pumping, a particularly promising direction is the generation of entangled rotatum arrays. For instance, nonlinear interactions could produce photon pairs that share not only an OAM state but also synchronized evolution. These correlations would evolve dynamically during propagation, enabling quantum key distribution with programmed entanglement and hybrid protocols spanning time, space, and OAM.

The roadmap ahead is defined by three directions. Metasurfaces provide a versatile physical layer, offering compact and efficient control of charge, polarization, and dispersion. Arrays of singularities supply the required complexity for computation, where coupling through diffraction, interference, and cavity feedback supports collective dynamics and scalable reservoirs. Finally, entangled rotatum arrays allow nonlinear interactions which can generate photon pairs with structured entanglement, yielding spatially engineered correlations. These developments inspire a future where light does not merely carry structure, but evolves with purpose towards fast, secure, and efficient information processing.

8 Longitudinal tailoring of singular optical beams and their applications (Alan E. Willner, Huibin Zhou, Yuxiang Duan, and Xinzhou Su)

8.1 Background

The ability to shape the spatial distribution of optical fields has given rise to a growing research area—structured light, which explores how light's spatial properties can be engineered and utilized in various applications [6]. This field blossomed in 1992 when L. Allen, et al. [50], showed that light beams with a helical phasefront and a vortex-like intensity profile can carry orbital angular momentum (OAM). Such beams fall under singular optics, which studies optical vortices and phase singularities that are present in many forms of structured light [6].

In general, any optical beam can be tailored to exhibit a unique transverse spatial structure by combining orthogonal transverse modes selected from a modal basis set. By applying complex coefficients to these modes, it is possible to synthesize an arbitrary transverse light field. A well known example is given by the Laguerre Gaussian modes $\mathrm{LG}_{\ell,p}$, where ℓ is the orbital angular momentum value that specifies the number of 2π phase changes in the azimuthal direction, and p is related to the number of radial intensity rings [6]. Transversely structured light has been demonstrated in communication, where orthogonal modes enable channel multiplexing and encoding to increase capacity, in sensing, where modal coupling can serve as a signature to extract object information, and in imaging, where tailored field distributions can enhance resolution [6].

Neglecting beam divergence, such transverse spatial distributions typically remain unchanged during propagation. However, light can also be pre-programmed to evolve longitudinally with propagation distance. In this chapter, we discuss advances in longitudinally structured light, its applications, and our future perspectives.

8.2 Concept of longitudinally structured beams

To achieve flexible longitudinal beam structuring, one approach involves manipulating the longitudinal wavenumber k_z, which naturally arises in Bessel-Gaussian modes BG_{ℓ,k_z} (see Fig. 6a1) [18]. The quantity k_z denotes the component of the light wave vector $\mathbf{k}$ along the propagation axis z (see Fig. 6(a2)). Different values of k_z correspond to different phase velocities of the beam along the propagation direction. A longitudinally structured beam can be created by a coherent superposition of multiple Bessel-Gaussian beams, each with a distinct value of k_z. By designing the complex coefficients of the different k_z components, it is possible to control their constructive and destructive interference (see Fig. 6(a3)) [51]. As a result, the beam exhibits higher on axis intensity at selected predesigned distances, while at other distances the on axis intensity is reduced.

In addition to intensity, longitudinal manipulation has also been demonstrated for other light properties, e.g., beam

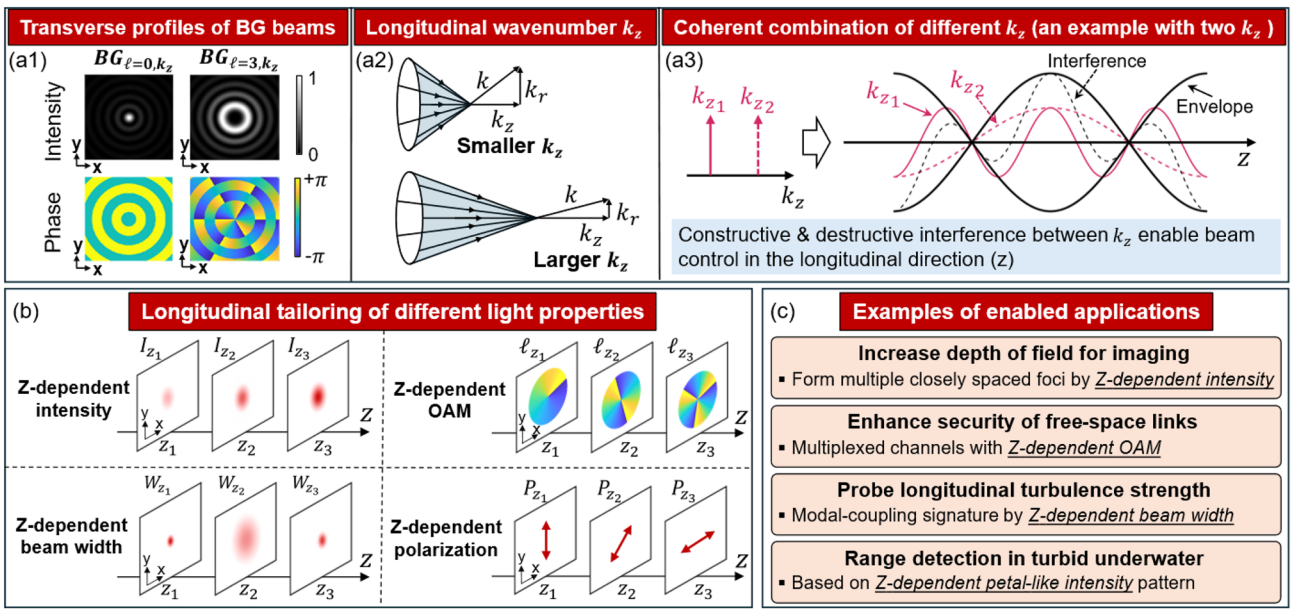

Fig. 6 **a1** Transverse profiles of two examples of Bessel-Gaussian beams BG_{ℓ,k_z}. **a2** The longitudinal wavenumber k_z, which is the component of the wave vector $\mathbf{k}$ along the propagation axis. **a3** Coherent combination of multiple k_z components enables beam control along the longitudinal direction. **b** Examples of longitudinal tailoring of different light properties. **c** Applications enabled by longitudinally structured beams

width, OAM value, and polarization (Fig. 6(b)). The underlying mechanism is similar: multiple LSBs, each carrying a distinct property, are combined so that a specific property emerges at a desired propagation distance [18, 51].

8.3 Applications of longitudinally structured beams

LSBs have the potential to enable a variety of applications [9], including (Fig. 6c):

(a) *Imaging with extended depth of field (DOF):* In microscopy, a conventional focused Gaussian beam often exhibits a shallow DOF, which limits the longitudinal imaging range. To address this limitation, a needle shaped longitudinally structured beam (LSB) has been demonstrated, where the on axis intensity is controlled to form multiple closely spaced foci along the propagation path. This approach can increase the effective DOF by more than ten times [9].
(b) *Enhancing the "security" of free– space communications:* The probability of intercept of free- space optical links can be reduced by transmitting data channels carried by different LSBs [9],. Each LSB is tailored to have a distinct OAM value that varies with distance. Therefore, only within a specific distance region can the data channels be detected by a legitimate receiver with low modal channel crosstalk [9].
(c) *Probing longitudinal turbulence strength:* Knowing the inhomogeneous spatial distribution of atmospheric turbulence is valuable in mitigating its negative effects. Multiple different LSBs can be transmitted sequentially to probe the turbulence strength along a path [9]. Each LSB has a distance-dependent beam width, resulting in distance-dependent OAM modal coupling caused by turbulence. Based on measured modal coupling effects, the distributed turbulence strength can be extracted.
(d) *Ranging in turbid underwater environments:* An LSB-based method has been demonstrated for underwater ranging [9]. The beam, composed of two BG modes with different OAM and k_z values, forms a petal-shaped transverse intensity pattern due to OAM mode interference. The two different k_z's induce a distance-dependent phase delay between the two modes, causing the petal to rotate during propagation. The distance can be determined by measuring this rotation angle.

8.4 Conclusions and future perspectives

LSBs hold various promising directions for future exploration. Topics include:

(i) *ntegrated approaches for LSB generation:* Developing low-size, weight, and power (SWaP) methods for LSB generation is critical for practical applications. Potential approaches include photonic integrated circuits and metasurfaces [18]. Key considerations involve beam purity, tunability, and scalability.
(ii) *LSB propagation in fibers:* Most LSB demonstrations have been performed in free– space. Extending LSBs to guided systems (e.g., optical fibers) presents new challenges, as the number of supported modes and wavenumbers may be limited [9]. Exploring how LSBs can be generated and propagated in fibers might be an intriguing research direction for new applications.
(iii) *Nonlinear light–matter interactions:* The distance-dependent control of LSBs could facilitate studies of longitudinally varying nonlinear light–matter interactions [6].
(iv) *Multi-dimensional synthesis:* Longitudinal beam structuring is closely related to temporal and transverse structuring. Manipulation across multiple dimensions might be possible, thereby enabling dynamic control of instantaneous 3D light states [9].

9 Orbitalization ellipsometry (Olga Korotkova)

9.1 Background

Seminal contributions by G. G. Stokes, H. Poincaré, R. C. Jones, and H. Mueller to the characterization of vectorial optical beams and their interactions with matter have laid the foundation for Polarization Ellipsometry (PE)—a technique now widely employed for sensing and imaging of polarization-sensitive media [52]. Beyond this, PE has also been adapted for use in communication systems involving polarization-insensitive media, where scalar light properties may fluctuate. For beam-like optical fields, polarization is inherently a local (point-wise) property, characterized by two orthogonal modes in physical space. The electric field, being a 2D isotropic oscillator, traces an ellipse known as the polarization ellipse. In the case of random beams, only a fraction of the total energy typically resides in the pure (fully polarized) state, necessitating the specification of the degree of polarization. The Stokes vector together with the Poincaré sphere serve as the powerful alternative for visualizing and analyzing such vectorial light fields. As we show here, it appears possible to develop a counterpart of PE in the orbital angular momentum (OAM) domain.

9.2 Methodology

Foundational studies on OAM-carrying light have primarily focused on single OAM-state harmonic beams [50]. Let us instead consider a beam capable of oscillating at multiple OAM states. At a fixed transverse cross-section, such a beam can be decomposed into its polar Fourier spectrum, whose coefficients form a vector with components $E_l(\rho)$, $l_{\min} \leq l \leq l_{\max}$, that depend on the radial coordinate but not on the polar angle. This vector, referred to here as the orbitalization vector, serves as the OAM– space analogue of the Jones (polarization) vector [53]. Unlike the local, 2D, physical-space-based Jones vector, the orbitalization vector (1) is non-local (radius-dependent), defined over the full beam cross-section; (2) resides in the Fourier domain; and (3) may contain any number of components, L, finite in measurements or potentially infinite in theory. According to Fourier theory, the orbitalization vector—representing an L-dimensional (LD) isotropic oscillator—must trace an elliptical trajectory in a plane within the LD space. The orbitalization ellipse exists for any L, with its form depending on the chosen radius. This enables the modeling, characterization, generation, and measurement of multi-state OAM-carrying beams through the proposed technique of Orbitalization Ellipsometry (OE), which interprets their geometric structure as arising from the superposition of individual OAM components.

Unlike in PE, where the ellipse lies in a plane and is quantified by three parameters, area, eccentricity, and orientation angle with respect to the laboratory frame, OE must involve additional parameters specifying the orientation of the orbitalization ellipse in the LD space. This task can be readily accomplished, even for large L, using efficient matrix methods such as singular value decomposition.

In the case of a random light beam the orbitalization vector must be self-correlated to form the orbitalization matrix, with elements $O_{lm}(\rho) = \langle E_l^*(\rho) E_m(\rho) \rangle$. The orbitalization ellipse can then also be uniquely determined from its elements and the degree of orbitalization can be defined [54]. Furthermore, it appears possible to develop a combined polarization-orbitalization ellipsometry using the recently introduced tensorial approach [55].

9.3 Experimental approach

We now outline an experimental procedure for measuring the elements of the orbitalization matrix via amplitude division interferometry (see Fig. 7). A laser beam that has interacted with a sample is split into two branches of a Mach-Zehnder system and recombined using a pair of beam splitters. Each branch, say, A and B, contains a spiral phase plate with OAM index l_n $(n = A, B)$, a ring aperture with radius ρ, and a Gaussian lens with focal length f. One branch also includes a π-phase plate to assess the imaginary part of the matrix elements. Precise symmetry of the branches and perfect alignment must be maintained to ensure robust interference. A CCD camera is placed after the beam combiner, exactly in the focal plane of both lenses. By recording the interference patterns for all contributing pairs of OAM indices and at all radii of interest, the elements of the orbitalization matrix can be measured. Due to its intrinsic symmetries (for example, Hermiticity), measurements of some elements can be omitted. Spiral plates, ring aperures and lenses can be also implemented by a pair of spatial light modulators (SLMs). By synchronizing the SLMs and the camera it appears possible to achieve automatized sequential measurement of the selected or all the matrix elements. Furthermore, by placing a polarizer in each branch, a quarter wave plate in one branch, and a compensating plate in the other, one can also measure ellipses as they appear in polarization-orbitalization tensor analysis [55].

9.4 Conclusions and future perspectives

Thus, we have introduced Orbitalization Ellipsometry (OE) as the counterpart of Polarization Ellipsometry (PE) in the OAM space and discussed a possible implementation of an interferometer for measuring the orbitalization matrix. This is not the only approach to such measurement; for instance, interferometry or holography can first be used to measure the complete 2D beam's cross-spectral density, followed by analytical calculation of the orbitalization matrix. However, our approach offers a direct yet selective method for accessing the individual elements of this matrix.

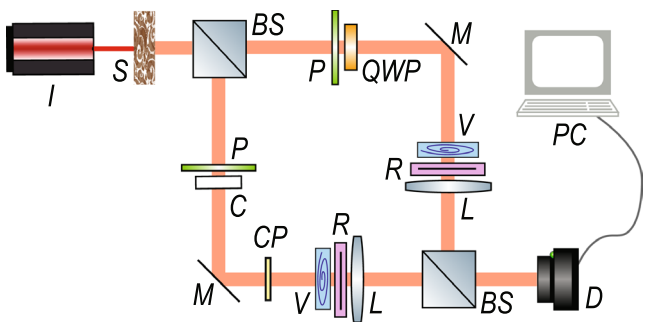

I: illumination source
S: sample
BS: beam splitter
P: polarizer
C: compensating plate
QWP: quarter-wave plate
M: flat mirror
CP: π-phase plate
V: spiral phase plate
R: ring aperture
L: convex lens
D: detector
PC: personal computer

Fig. 7 Mach-Zehnder interferometer for orbitalization ellipsometry measurements

Since the orbitalization ellipse carries the signature of a deterministic or random medium with which the beam interacted—reflecting angular phase asymmetries, vorticity, phase dislocations, etc.—it is envisioned as a sensitive diagnostic tool for optical metrology and remote sensing. This is particularly relevant for polarization-insensitive natural media, such as atmospheric and oceanic turbulence, certain biological tissues, as well as some natural rough surfaces and particulate collections. In addition, the combined polarization–orbitalization ellipse measurement would complete the description of light's signature across all possible structured states.

10 Retrieving nanoscale orientation and shape anisotropy via spin–orbit light conversion (Petr Bouchal, Petr Viewegh, and Zdeněk Bouchal)

10.1 Background

Determining the three-dimensional (3D) orientation and shape anisotropy of nanoscale objects is an essential task in nanoscience, with applications ranging from single-particle tracking and nanoantenna characterization to understanding structural organization in complex materials and biological systems. A range of techniques, such as polarization-resolved fluorescence microscopy, defocused imaging, and engineered point spread functions, have been developed to extract orientation information beyond the diffraction limit [56]. Other methods, including interferometric scattering and holographic approaches, can provide access to nanoscale geometry through correlations of scattered and unscattered light [57]. Although these approaches have been successful, they are frequently constrained by trade-offs between spatial resolution, acquisition speed, and experimental simplicity.

In this context, we have developed and demonstrated a far-field optical approach based on spin–orbit conversion of scattered light [58], which enables access to the 3D orientation [59], and aspect ratio [60], of individual, optically unresolved nano-objects. This strategy relies on manipulating the angular momentum of scattered light through its geometric (Pancharatnam-Berry) phase, resulting in far-field signatures that reflect the object's symmetry and orientation. Notably, the method bypasses polarization scanning and remains compatible with standard wide-field microscope configurations, making it broadly accessible to darkfield and fluorescence imaging.

10.2 Methodology

To illustrate the method, a nano object with a high aspect ratio and a 3D orientation defined by the azimuthal and polar angles θ_0 and ϕ_0 is considered (Fig. 8a). This nano object represents a radiating dipole, with its dipole moment $\vec{\mathbf{p}}$ conveniently decomposed into components $\vec{\mathbf{p}}_L$ and $\vec{\mathbf{p}}_A$, oriented laterally (in the xy plane) and axially (along the z axis). The electric fields $\vec{\mathbf{E}}_L$ and $\vec{\mathbf{E}}_A$ of the scattered light, originating from $\vec{\mathbf{p}}_L$ and $\vec{\mathbf{p}}_A$, correspond to lateral and axial orientations of the nano object, and will therefore be referred to as the lateral imaging mode (LIM) and axial imaging mode (AIM) (Fig. 8b). The resulting electric field of the scattered light is given by $\vec{\mathbf{E}} = A\vec{\mathbf{E}}_L + B\vec{\mathbf{E}}_A$, where A and B depend on ϕ_0. The LIM is expressed as a superposition of right and left handed circular polarizations $\vec{\mathbf{J}}_R$ and $\vec{\mathbf{J}}_L$, with the phase retardation that depends on θ_0, $\vec{\mathbf{E}}_L = e^{-i\theta_0}\vec{\mathbf{J}}_R + e^{i\theta_0}\vec{\mathbf{J}}_L$. The AIM exhibits spatially varying polarization, formed by circularly polarized vortex beams with topological charges $m = \mp 1$, $\vec{\mathbf{E}}_A = e^{-i\theta}\vec{\mathbf{J}}_R + e^{i\theta}\vec{\mathbf{J}}_L$. As a result, $\vec{\mathbf{E}}_A$ oscillates radially at each azimuthal position θ. Thus, the in plane nano object orientation θ_0 is embedded in the superposition of light states with spin angular momentum (SAM), while its out of plane tilt ϕ_0 is encoded in the states carrying both SAM and orbital angular momentum (OAM). To imprint the information about θ_0 and ϕ_0 into the detected intensity pattern, the LIM and AIM are transformed by a spin–orbit coupling matrix, defined by rotation matrices as $W = R_{-\theta/2}\ \mathrm{diag}(1,-1)\ R_{\theta/2}$. The action of W on the circular polarizations $\vec{\mathbf{J}}_R$ and $\vec{\mathbf{J}}_L$ changes their handedness and generates a geometric vortex phase with topological charges $m = \pm 1$, constituting a spin–orbit interaction that reverses SAM and induces OAM. In the experiments, light scattered by the nano object is collected by a microscope objective and directed onto a half wave plate with spatially varying anisotropy axis, called a q-plate, which implements the matrix W [59]. The LIM transformed by the q-plate acquires a vortex phase, $\vec{\mathbf{E}}_L \propto R_L\left[e^{-i(\theta-\theta_0)}\vec{\mathbf{J}}_R + e^{i(\theta-\theta_0)}\vec{\mathbf{J}}_L\right]$, where R_L describes the annular amplitude profile typical of the vortex beam. After polarization projection to the direction $\alpha = 0$, the detected intensity $I_L \propto |R_L|^2 \cos^2(\theta - \theta_0)$ forms a double helix point spread function (DH PSF), whose lobes uniquely determine the azimuthal orientation θ_0 of the nano object (Fig. 8(c, top)). By transforming the AIM with the q-plate, the vortex phase is fully compensated, and after polarization projection, the resulting intensity $I_A \propto |R_A|^2$ corresponds to an Airy disk (Fig. 8(c, bottom)). The DH PSF and the Airy disk are obtained only when the nano object is in the lateral ($\phi_0 = \pi/2, B = 0$) or axial ($\phi_0 = 0, A = 0$) position. For a general nano object orientation, the DH PSF and Airy disk combine with weights depending on ϕ_0, resulting in an optical footprint from which θ_0 and ϕ_0 can

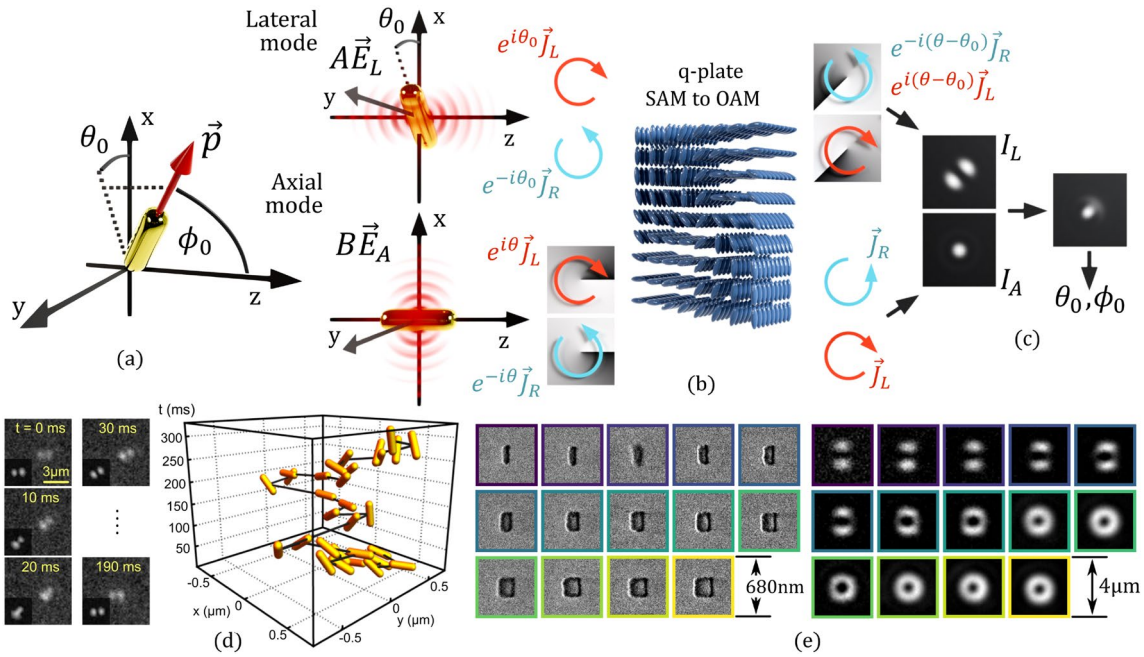

Fig. 8 Orientation and shape anisotropy imaging via SAM-to-OAM conversion. **a** 3D orientation of a dipole moment given by azimuthal and polar angles, θ_0 and ϕ_0. **b** Lateral and axial imaging modes using SAM-to-OAM conversion to encode 3D dipole orientation into the image spot. **c** DH PSF (lateral mode) and Airy disk (axial mode), and their superposition forming a structured pattern. **d** 3D orientation tracking of a gold nanorod at a frame rate of 100 Hz. e) Shape anisotropy of nanoparticles encoded into vortex images. Adapted from [59, 60]

be accurately extracted (Fig. 8(c, right)). In this way, the 3D orientations of all nano objects within the field of view are simultaneously retrieved, achieving high temporal resolution (Fig. 8d).

10.3 Results

The method was successfully applied to 3D orientation imaging of gold nanorods with a high aspect ratio (70×25 nm). These nanorods exhibited dominant longitudinal surface plasmon resonance, characterized by a dipole moment aligned with their long axis. The scattered light was filtered from the illumination using dark-field microscopy, and the 3D orientation of the nanorods was reconstructed by correlating the measured data with a library of theoretical PSFs. The method was calibrated by imaging the azimuthal orientation of artificial nanorods fabricated using electron beam lithography. In advanced experiments, the 3D orientation of colloidal nanorods was measured during their Brownian motion (Fig. 8d) or interaction with cellular membranes. The imaging speed was limited only by the signal-to-noise ratio, and we achieved frame rates up to 500 Hz [59].

We used a method beyond 3D orientation imaging, demonstrating its sensitivity to the shape of nanoparticles. More symmetrical nanoparticles can support lateral and longitudinal surface plasmon resonance of comparable strength, creating two perpendicular dipole moments. The superposition of DH PSFs corresponding to these perpendicular dipole moments shapes the resulting PSF and encodes the nanoparticle aspect ratio [60]. The measurement was successfully calibrated against scanning electron microscopy (Fig. 8e).

10.4 Conclusions and future perspectives

The SAM-to-OAM conversion method proved advantageous compared to traditional methods that rely on strong defocusing of detected signals and demonstrated practical relevance. The improved signal-to-noise ratio can be beneficial for extending the approach to fluorescence imaging. In this context, fluorescent nanoparticles exhibiting quantum confinement effects or atomic vacancies enabling single-photon emission could serve as suitable samples for further investigation.

11 Measuring topological charges of vortex beams (Allarakha Shikder, Mansi Baliyan, Praveen Kumar, and Naveen K. Nishchal)

11.1 Background

Optical vortex beams, characterized by phase singularities and orbital angular momentum (OAM), are fundamental entities in singular optics. Their unique wavefront structure

enables diverse applications in imaging, manipulation, cryptography, and communications [8]. Beyond single vortex, structured arrangements such as optical vortex lattices provide enhanced control over light–matter interactions [61]. Another frontier in singular optics is the measurement of topological charges (TCs), which represent winding numbers in the helical phase front [62]. The value of the TC of a vortex beam can be an integer or a fraction. Accurate generation and measurement of vortex beams with integer or fractional TCs are essential for advancing singular optics research and its applications [63]. For fractional vortex beams, the value of TC is not uniquely defined rather depends critically on the measurement method and the propagation regime [64]. It has been theoretically shown that a Gaussian beam with an embedded optical vortex with original fractional TC does not conserve the original TC upon propagation [65]. Near-field observations may reveal fractional or transitional TC values, whereas far-field measurements often exhibit integer-like outcomes as a consequence of vortex evolution during propagation [66]. In practical implementations involving finite Gaussian beams encoded on spatial light modulators, beam waist size, truncation, and diffraction further modify the observable phase-singularity structure [64, 67]. These factors give rise to complex vortex dynamics, including the birth, annihilation, and migration of phase singularities, which manifest as ambiguities in the commonly reported TC 'staircase' behaviour [68].

The measurement of the TC of the vortex beam has been performed with manual analysis of interference or diffraction patterns by observing the changes occurring in the intensity patterns due to the change in TC [61]. However, in case of a vortex beam with fractional TCs in the near-field regime, the change in the interference fringe pattern is very minimal, creating difficulty in the quantification of fractional TCs. Non-interferometric convolution-based method for the generation of different types of optical vortex lattices and different methods for measuring fractional TCs using well-defined interference patterns is the need of the hour for future growth of the subject.

11.2 Methodology

Mathematically, the electric field distribution of a vortex beam at $z = 0$ can be expressed as [61]

$$U(x, y; l, \delta) = U_0(x, y; \delta)\ \exp\big(il\phi\big), \tag{13}$$

where $U_0(x, y; \delta)$, l, δ, and ϕ denote the intensity distribution of the beam in the x–y transverse plane, the TC, the coherence width of the light source, and the azimuthal coordinate, respectively. The phase only function (POF) required to generate this type of vortex beam can be expressed as [61]

$$P(l; x, y) = \Im[\log\{U(l; x, y)\}]\,, \tag{14}$$

where $\Im$ denotes the imaginary part of the complex function. If $N(x, y)$ is a lattice pattern function corresponding to any symmetry then the POF for generating an optical vortex lattice corresponding to that symmetry can be mathematically expressed as [61]

$$P_N(x, y) = P(l; x, y) * N(x, y), \tag{15}$$

where $*$ denotes the convolution operation between $P(l; x, y)$ and $N(x, y)$. The lattice pattern function $N(x, y)$ is a binary matrix. The light beam modulated by this POF, $P_N(x, y)$, will hold an array of vortices of TC $= l$ corresponding to each high value point of $N(x, y)$. Control of different properties of vortices in the array, for example TC values, geometries of vortices, and distance between two vortices, can be achieved by manipulating the lattice pattern function.

The interference between a vortex beam of TC l and a tilted Gaussian beam results in a fork shaped interference pattern. Such a tilted Gaussian beam can be mathematically expressed as [63]

$$\begin{aligned} E(x, y) = E_0(x, y)\exp\left\{-ik\frac{x^2 + y^2}{2R}\right\} \\ \exp\ \left[-ik\left\{x\sin(\alpha)\cos(\beta) + y\sin(\alpha)\sin(\beta)\right\}\right], \end{aligned} \tag{16}$$

where E_0 denotes the amplitude, k denotes the wavenumber, R denotes the radius of curvature of the wavefront, and α and β denote the tilt angles along the x axis and azimuth direction, respectively. The orientation and the width of the fork petals can be controlled by changing the values of α and β. The magnitude of the TC of vortices indicates the number of fork petals created in the interference fringe. If the sign of the TC becomes opposite, then the orientation of the fork petals rotates by an angle of $180°$, which helps to identify the sign of the TC.

11.3 Results

The schematic diagram of the experimental setup used for the generation of different types of arrays of vortices using a partially coherent light source, a light emitting diode is shown in Fig. 9a. For the generation of fork-shaped interference fringes corresponding to a vortex beam, the beam dump (indicated as component 'A' in Fig. 9a) is replaced by a tilted mirror. Figure 9b shows the phase and intensity distribution of different types of arrays of vortices.

In the near-field regime, if the vortex beam under examination contains a fractional TC, then an intensity dislocation line will be present at the singular point of the interference

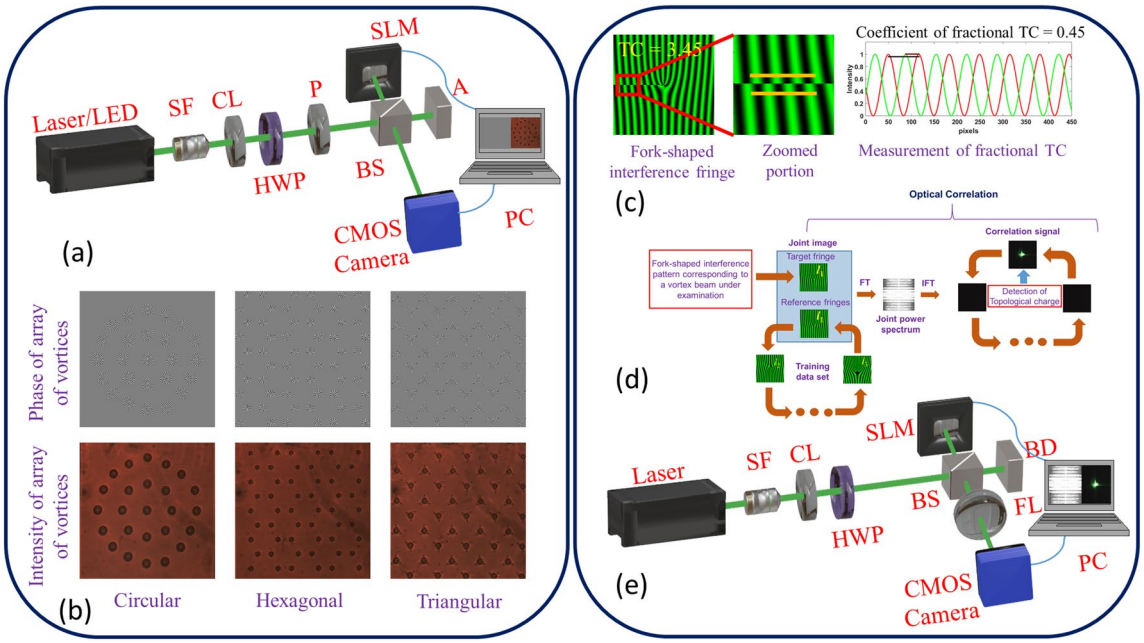

Fig. 9 **a** Schematic diagram of experimental setup for generation of an array of vortices, **b** intensity and phase distributions of an array of vortices, **c** fork-shaped interference patterns of vortex beam of TC = 3.45, **d** flowchart, and **e** schematic diagram of experimental setup for TC measurement using optical correlation method. SF: Spatial filter, CL: collimating lens, BS: Beam splitter, SLM: Spatial light modulator, CMOS: Complementary metal-oxide semiconductor camera, FL: Fourier lens, A: beam dump

fringe, depending on the phase profile of the light beam. Figure 9c shows the fork-shaped interference fringe patterns corresponding to a vortex beam of TC = 3.45 and the measurement of fractional TC using the intensity distribution along two lines (red and green) just above and below the intensity dislocation. The peak-to-peak distance between the red and green indicates the fringe-shift, and the peak-to-peak distance between the red lines represents the width of a single fringe; the ratio of these two distances represents the coefficient of fractional TC. For fractional TCs, fractional values do not contribute to the creation or annihilation of new fringes, creating difficulty for measurement through direct observation of the interference pattern. In this case, the fork-petals above and below the dislocation line is displaced by an amount based on the fractional value present in the beam, allowing quantification of the fractional TC through the analysis of fringe displacement [62]. The amount of fractional TC is equal to the coefficient of fractional TC, which is defined by the ratio of the fringe displaced above and below the dislocation line to the width of a complete fringe. Such a manual analysis of the interference fringe is time-consuming and becomes difficult in case of a beam with a larger TC values due to the increase in fringe density.

To overcome the limitation caused by manual analysis, an optical correlation-based TC measurement method is proposed, where the interference fringes obtained from the beam under examination is correlated with a reference fringe and the quantification is done based on the intensity of the correlation output [63, 69]. For real-time TC measurement, an optical correlation process is preferred. The flowchart and schematic diagram of the TC measurement process using optical correlation are shown in Fig. 9d and e, respectively. The method involves generating fork-shaped interference patterns for TC values ranging from -15 to +15 and using them as a minimal training dataset. The interference pattern of a test vortex beam is then optically correlated with this dataset via a hybrid digital-optical correlator setup and the TC is identified from the fringe pattern that yields the maximum correlation output.

11.4 Conclusions and future perspectives

It has been demonstrated that vortex lattices can be flexibly generated with partially coherent light sources using the convolution-based non-interferometric method. For TC measurement, the interference-based technique provided high-resolution characterization of fractional vortices, while the correlation approach enabled rapid and automated retrieval. Together, these results establish a versatile framework for generating complex vortex structures and measuring their topological properties. These advances enrich the singular optics toolkit and pave the way for broader applications.

Future research may focus on extending convolution-based methods to polarization and spatio–temporal singularity lattices while also integrating correlation-based TC detection with adaptive optics to compensate for turbulence. In addition, realizing vortex lattice generation and corresponding TC measurements at terahertz and infrared wavelengths remain an important direction, alongside the development of compact integrated devices for efficient on-chip vortex beam manipulation.

12 Extracting the spatial modes through intensity auto-correlation technique (Md. Haider Ansari, Ganesh Velagala, Sakshi Choudhary, Ravi Kumar, and Salla Gangi Reddy)

12.1 Background

Vortex beams are a significant milestone in contemporary optical sciences, driven by key scientific breakthroughs and rapid technological progress [21]. These beams are characterised by a phase singularity at their centre and carry well-defined orbital angular momentum (OAM) of $l\hbar$, l being the topological charge (TC) defined as the number of windings per wavelength. Their unique properties such as phase singularity, helical wavefront, and doughnut-shaped intensity distribution have made them to utilize in various applications such as free– space optical communication, high-dimensional information encoding, optical manipulation, and imaging [20, 50, 70]. The singularities have been realised in both coherent and partially coherent optical beams. When vortex beams propagate through atmospheric turbulence or other scattering media, they become partially coherent and leads to the formation of a random optical pattern called speckles [71–73]. These random fields can also be produced by scattering a coherent beam through a rough surface, such as a ground-glass plate (GGP). Scattered optical fields are becoming increasingly important in science and technology due to their applications in communication, cryptography, and optical manipulation. In spatial-mode-based free– space optical communication, the TC of the optical vortex is a crucial parameter that can act as an information carrier for transmitting the data [74–77]. Studies indicate that vortex beams are resilient against atmospheric turbulence and can travel longer distances without losing OAM information [78, 79]. Therefore, it is vital to accurately diagnose the TC even after the beam propagates over extended distances or through scattering media. Several techniques have been proposed to measure the TC of coherent optical vortices [80–82]. However, these methods fail when a vortex beam is disturbed by atmospheric turbulence or by scattering media, as the field pattern and phase singularity are compromised. Incorrect TC measurements can lead to increased bit-error rates and reduced channel capacity in optical communication systems [10]. To address the limitations of traditional TC measurement techniques, we demonstrated a straightforward, non-interferometric intensity autocorrelation-based method for assessing and quantitatively measure the TC of both integer- and fractional-TC vortex beams (FOV). The area of scattered autocorrelation intensity profiles and the divergence of dark-ring radii with increasing propagation distance observed in these profiles is used to determine the spatial mode of vortex beams. Furthermore, our method is independent of the beam waist used to generate the vortex beams. These results provide the characterization of phase profiles with the help of intensity measurements.

12.2 Methodology and results

The optical vortex beams are scattered through a ground glass plate (GGP) and then the perturbed optical beams, that is speckle patterns, are recorded. The field distribution of optical vortex (OV) beams can be represented mathematically as

$$E(\rho,\theta,0) \propto \rho^{|m|} \exp\left(-\frac{\rho^2}{\omega_0^2}\right) \exp\big(im\theta\big), \tag{17}$$

where ω_0 is the beam waist and (ρ,θ) are cylindrical coordinates at the vortex generation plane. The scattering of OV beams through a GGP can be well modelled with a δ correlated random phase function, where Φ varies randomly from 0 to 2π and can be obtained by taking a two dimensional convolution between a random spatial function and a Gaussian correlation function. The field distribution of speckles obtained after scattering through the GGP is given by

$$U(\rho,\theta) = \exp\big(i\Phi\big)\, E(\rho,\theta,0). \tag{18}$$

The auto correlation function between two speckle patterns of the same TC obtained by scattering OV beams through a GGP is given by

$$\Gamma(r_1,\varphi_1;r_2,\varphi_2) = \big\langle U_1(r_1,\varphi_1)\, U_2^*(r_2,\varphi_2)\big\rangle, \tag{19}$$

where $\langle a\rangle$ denotes the ensemble average operation of the parameter a, and (r,φ) are the coordinates at the detection plane. After solving the Fresnel integral, the correlation function is obtained as [10, 83]

$$\Gamma_{12}(\Delta r) = \frac{\pi \omega_0^{2|m|+2}(|m|)!}{2^{|m|+1}\lambda^2 z^2} \exp\left[i\frac{k}{2z}(r_1^2 - r_2^2)\right] \exp\left(-\frac{k^2\omega_0^2\Delta r^2}{8z^2}\right) L_{|m|}\left(\frac{k^2\omega_0^2\Delta r^2}{8z^2}\right), \tag{20}$$

where $L_{|m|}(\cdot)$ denotes the Laguerre polynomial of order $|m|$.

The autocorrelation function of perturbed optical vortices is therefore given by a Laguerre polynomial of order m, and the number of zero points is equal to the order m. From these zeros one can extract information about the spatial mode. It is known that the Fourier transform of the incident field can represent the autocorrelation function, and the Fourier transform of a coherent optical vortex has m zero points. Observation of these zero points in experiment is difficult because the correlation strength decreases with spatial separation. To avoid this limitation, one can consider the lowest root of the Laguerre polynomial, and define the correlation length as the value of Δr at which the correlation vanishes. It can be written as

$$\Delta r_0 = \frac{\sqrt{8c_m}}{k\omega_0} z, \tag{21}$$

where c_m is the lowest root of the corresponding Laguerre polynomial. From Eq. (21), the correlation length is directly proportional to the propagation distance z. Mathematically, the variation of correlation length with z can be written as

$$\alpha = \frac{\partial \Delta r_0}{\partial z} = \frac{\sqrt{8c_m}}{k\omega_0}. \tag{22}$$

Experimentally, one can find the divergence α as the slope of Δr_0 versus z, and this quantity is independent of the propagation distance. This information can be combined with known input parameters, such as wavelength and beam waist, to determine the TC of a perturbed vortex.

This theory is valid for both integer and fractional charge scattered vortex beams. OV beams are generated by modulating the laser beam with a computer generated hologram displayed on a liquid crystal device, that is a spatial light modulator. Figure 10a displays the autocorrelation profiles obtained for experimental speckles (top) and the theoretical results (middle) along with the corresponding speckle patterns (bottom). Figure 10b shows the autocorrelation intensity profiles of fractional TC values $m = 1.2$, 1.5, and 1.8.

From Fig. 10, it is clear that the number of rings present in the autocorrelation is equal to the TC in the integer vortex beams and for fractional vortex beams the new ring starts evolving with the increase in fraction towards the next integer. It is also noted that for the integer TCs, the rings are symmetric, well-defined dark ring structures. However, for FOV beams, asymmetric ring structures appear in the autocorrelation profiles, with the number of rings approximately equal to the TC rounded to the nearest integer. This method works very well for vortices with low TC; however, for large TC observing many dark rings is difficult due to reduced correlation strength. To overcome this challenge, we used the divergence of the first dark ring radius to measure higher-TC vortices, since the first dark ring can be observed even for higher TCs and at all the propagation distances. The divergence is defined as the rate of change of the first dark ring with respect to propagation distance. The radius of the first ring and its divergence as a function of TC are shown in Fig. 11. The experimental and theoretical results are in good agreement with each other which will make us to utilize this property for the diagnosis of TC. The similar results are obtained for FOV beams. It is observed that the radius and the divergence decrease with the increase

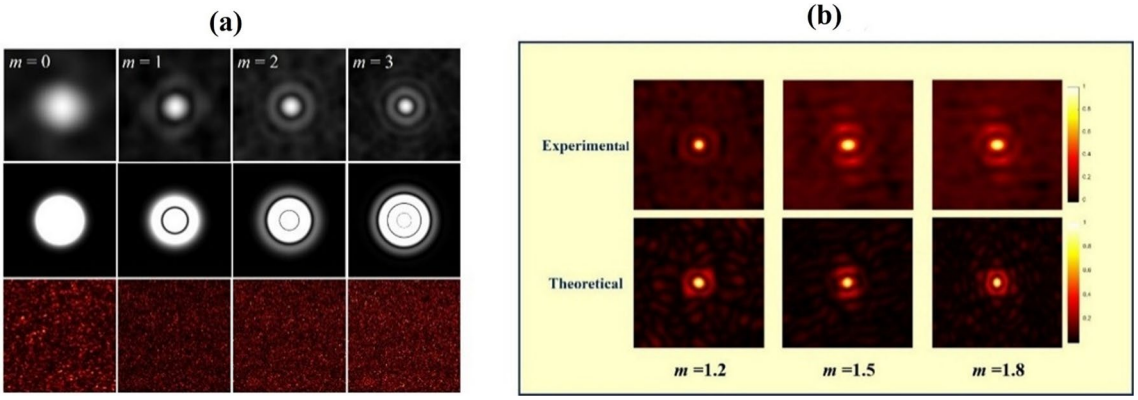

Fig. 10 **a** Experimentally obtained autocorrelation profile (first row), the theoretical results (second row), and the corresponding speckles (third row) for integer vortex beams with $m = 0, 1, 2, 3$ from left to right at a propagation distance of $z = 25$ cm. **b** Experimental (first row) and theoretical (second row) intensity profiles for fractional vortex beams with $m = 1.2, 1.5,$ and 1.8 at a propagation distance of $z = 25$ cm

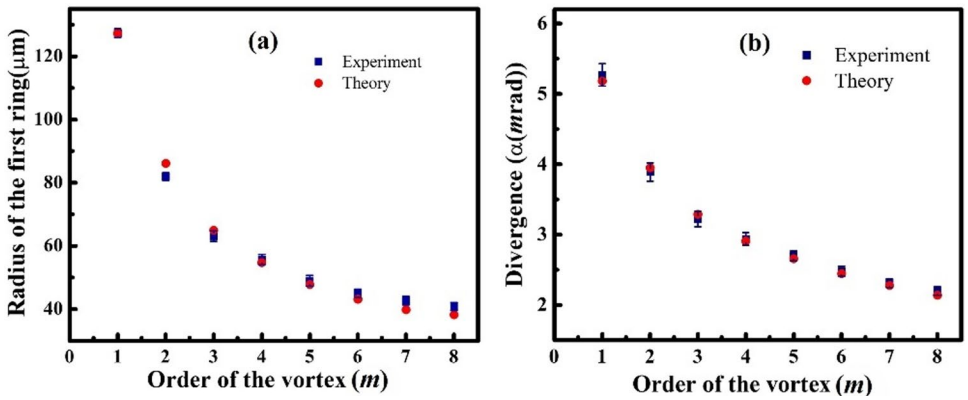

Fig. 11 Experimental (blue) and theoretical (green) variation of radius of the first dark ring **a** and its divergence variation **b** with the TC of the OV beam

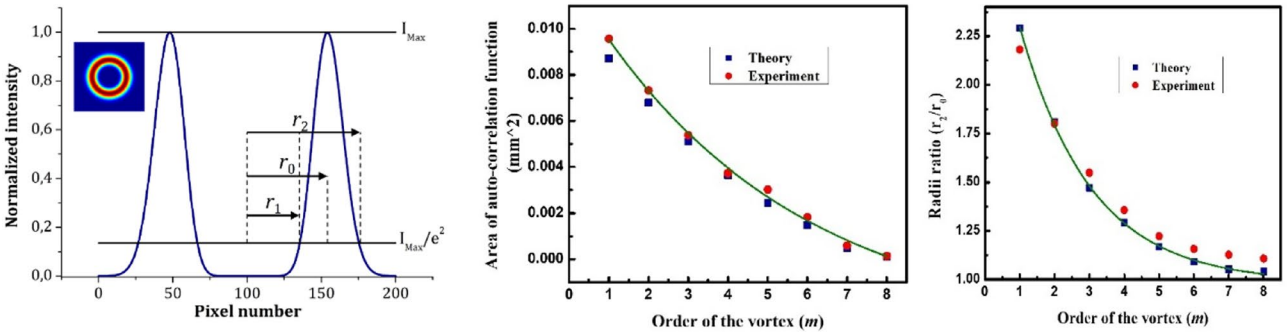

Fig. 12 Transverse intensity profile and the line profile (left) for an OV beam with TC $m = 10$, area of auto-correlation profile (middle) and the radii ratio (right) as a function of TC m

in TC. However, the results depend on the parameters used to generate the OV beams such as beam waist.

Now, we proceed with the development of autocorrelation-based technique which is independent of initial parameters used to generate OV beams. The intensity distribution of OV beams and the corresponding line profile is shown in left of Fig. 12. From the simulation, it has been shown that the ratio of two radii r_2/r_0 of a coherent vortex and the area of the autocorrelation profile of the scattered OV beams show the similar behaviour.

The middle image in Fig. 12 shows the variation of area correlation functions A_m and right image shows the variation of radii ratio r_2/r_0. From these two, we observe that both exhibit a negative exponential behaviour. This identical behaviour, we established a relation between A_m and R_m given as $R_m = 146.8 \times 10^6 A_m + 1.024$ [84] which does not depend on the beam waist and provides a simple method to find the TC of any vortex, regardless of its beam waist.

12.3 Conclusions and future perspectives

In conclusion, we demonstrated that the spatial mode of vortex beams can be reliably identified using only the intensity autocorrelation of their scattered speckle fields. For lower TC vortices, the number of dark rings in the 2-D autocorrelation map directly indicates the TC. For higher TC, the divergence of the first ring offers a robust alternative, especially when ring visibility diminishes due to low coherence. Additionally, by analysing the area of the autocorrelation function, we used a simple method to determine the TC, independent of the beam waist, even with small speckle patterns. These findings emphasise that autocorrelation is a powerful, non-interferometric technique for characterising perturbed, integer, and fractional vortex beams. The potential applications include free– space and satellite communication, ghost imaging, optical encryption, and data authentication.

Even though the proposed method is highly robust, future research could focus on enhancing its performance in stronger turbulence and applying it to multimode, vector, or more complex structured beams. Investigating new types of structured light and varying scattering conditions may improve the sensitivity and stability of autocorrelation features. Combining this method with compact platforms such as SLMs, metasurfaces, or on-chip photonic devices could lead to portable, efficient OAM analysers. Additionally, employing machine-learning techniques to analyse autocorrelation profiles might enable accurate mode extraction from very small or heavily distorted speckle regions. Ultimately, these developments could set intensity autocorrelation as a simple, reliable, and practical method for future

structured-light applications. Further, one can improve these techniques for the development of demultiplexing schemes where one needs to find the TC of all the multiplexed OV beams.

13 Progression of speckle-learned structured light detection from 2D camera to 0d single-pixel fast photodiode (Purnesh Singh Badavath and Vijay Kumar)

13.1 Background

The detection of structured light beams such as orbital angular momentum (OAM), Hermite–Gaussian (HG), and more complex light beams has become a central challenge in modern optics. Traditional methods based on imaging or interferometric diffraction require complex optics, precise alignment, and large data acquisition. Speckle-learned Recognition (SLR) offers a new paradigm by exploiting the random yet information-rich speckle patterns produced when structured light interacts with scattering media [85]. Instead of reconstructing the beam, SLR uses machine learning to search for the structured light information within the speckle patterns. It enabling compact, alignment-tolerant detectors that remain robust in noisy environments. By mapping structured light's 2D spatial information onto 2D speckle images [85, 86], 1D spatial speckle arrays [86, 87], and 0D temporal speckle sequences [88, 89], SLR is revolutionizing structured light detection (Fig. 13).

13.2 Methodology

In free– space, the propagated structured light beam interacts with the random media such as rotating diffuser to generate the spatio– temporal speckle field. The spatio– temporally varying speckle fields, while random in appearance, are rich in information about the scattered beam and serve as the raw data for subsequent detection in spatial and temporal domains.

A 2D camera is typically used to capture speckle pattern images, providing high accuracy but at the cost of large data volumes and slower acquisition due slower frame rates. To over come this bottleneck, a 1D line camera is employed to capture the spatial fluctuations, which reduces the data load to about one-nth of that in 2D SLR, while still having the essential information needed for structure light detection. In addition to structured light detection in spatial domain, 0D SLR has also been introduced, where a single-pixel fast photodiode records temporal speckle fluctuations directly in time. This approach operates at ultrafast rates, making it particularly promising for high-speed communication and sensing scenarios.

For classification, coustom-designed deep learning models trained on the captured speckle data in spatial and temporal domains are employed. A 2D convolutional neural network (CNN) is typically used for spatial recognition with 2D speckle image. As the captured data dimentionality and the inherent 2D camera's slow frame rates adds delay to high-speed structured light detection. Where as 1D CNN architectures are more suitable for handling the reduced-dimension data for 1D SLR. Promising reduced data, training time, and computation overhead than 2D SLR. The physical data dimensionality reduction not only lowers the training data requirements but also accelerates the capturing

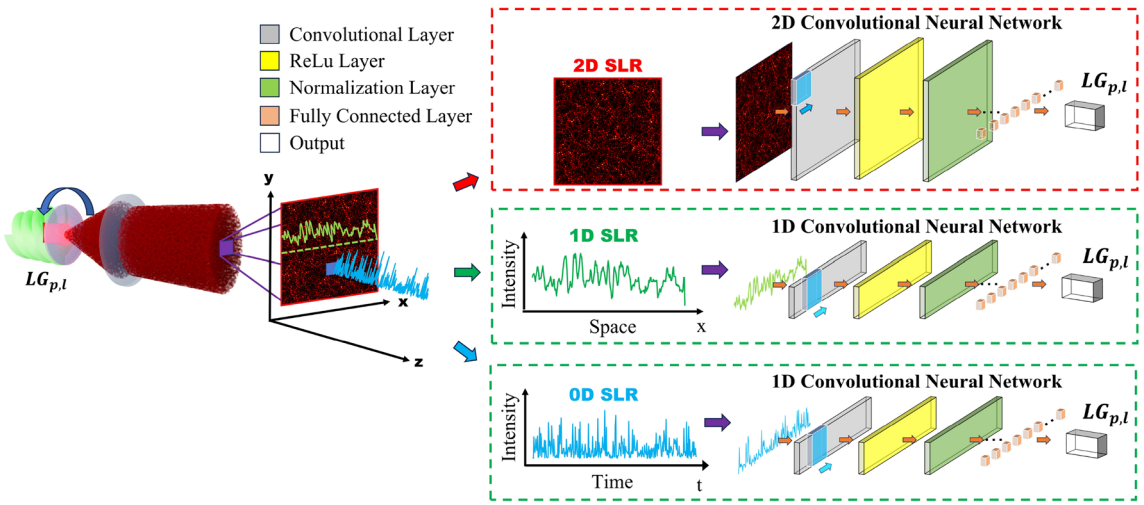

Fig. 13 Progression of speckle-learned structured light detection using 2D speckle images, 1D spatial speckle array, and 0D temporal speckle sequences

and detection speed. In 1D SLR, recognition speed remains limited by the need for synchronized spatial detectors, even though the data volume is smaller than in 2D SLR. By contrast, 0D SLR employs a single-pixel detector that captures temporal fluctuations at much higher rates. Combining faster data acquisition and classification using 1D CNN, significantly accelerate structured light detection.

13.3 Results

Initial demonstrations of 2D SLR using speckle images have achieved near-perfect classification of OAM and HG beams exceeding 96% classification accuracy [85, 86]. However, the reliance on large data volumes and camera frame rates limits their speed and scalability. The 1D SLR, employing spatial speckle array, the classification accuracy remains high at 94% while reducing the data requirement to a fraction of the 2D SLR [86, 87]. For OAM beams subjected to turbulence, 1D SLR has achieved an classification accuracy of 79%. The most robust approach, 0D SLR, leverages temporal speckle sequences recorded by a single-pixel fast photodiode [88, 89]. Remarkably, this method achieves classification accuracies of 96% for intensity degenerate OAM modes and maintains robustness even in severe turbulent conditions, where camera-based methods often fail. By drastically reducing dimensionality, 0D SLR accelerates recognition, minimizes storage and training time, and enables real-time classification, making it the fastest and most scalable strategy reported to date.

13.4 Conclusions and future perspectives

Structured light detection has become a cornerstone for both research and industrial applications, driving advances in high-capacity communication, precision sensing, imaging, and secure information processing. Its importance lies in the ability to reliably identify and classify complex optical fields, a task that traditionally demanded elaborate optical setups and heavy computation. SLR transforms this challenge into an opportunity by harnessing spatio–temporal speckle dynamics, enabling compact, fast, and scalable detection across multiple dimensions. By progressively mapping structured light 2D spatial information onto 2D speckle images to 1D spatial speckle arrays and finally to 0D temporal speckle sequences, it delivers remarkable gains in efficiency and speed without compromising accuracy, making structured light detection more practical for real-world deployment.

Looking ahead, research can extend the impact of SLR by scaling it to hundreds of spatial modes for high-capacity optical communication, integrating the approach into chip-scale platforms for compact and alignment-free devices, and harnessing neuromorphic or photonic processors to achieve real-time recognition. Beyond communication, its potential also reaches into secure authentication, advanced sensing, and low-light quantum networks, opening new directions for practical and versatile optical technologies.

14 Optimal receiver strategies for OAM beams via sampled detection (Ayush Mehra and Shlomi Arnon)

14.1 Background

Light beams carrying Orbital Angular Momentum (OAM) have attracted significant attention in optical communication, quantum information, and optical metrology. Their helical phase structure provides a theoretically unbounded set of orthogonal states, which can be harnessed for multiplexing and encoding information beyond the limits of polarization and wavelength [12]. This additional degree of freedom has motivated diverse applications ranging from high-capacity communication links to structured-light sensing and quantum entanglement experiments.

A fundamental challenge in exploiting beams carrying OAM lies in their detection and sampling. Unlike Gaussian beams, OAM modes diverge more rapidly with propagation, resulting in large spot sizes at the receiver plane. Conventional receivers therefore require capturing the full beam cross-section with large optics, which leads to bulky hardware, stringent alignment requirements, and limited integration with chip-scale devices [90]. These constraints affect free– space optical communication as well as fiber communication and photonic integrated circuits where compact OAM receivers are essential.

This challenge becomes particularly severe in long-distance optical communication, including satellite-to-satellite and deep– space systems, where diffraction-induced divergence and pointing errors demand impractically large apertures for full-beam capture [91]. Overcoming this limitation requires innovative receiver-side strategies capable of extracting reliable information from only a portion of the OAM beam, without relying on full-beam detection.

14.2 Current state-of-the-art

Over the past decade, significant progress has been achieved in addressing the limitations of orbital angular momentum (OAM)-based optical communication. Conventional approaches typically rely on capturing the

full spatial extent of the OAM beam, a requirement that becomes impractical in long-distance space applications where diffraction-induced divergence produces excessively large spot sizes at the receiver. To overcome this limitation, researchers have investigated partial-aperture detection, in which only a fraction of the OAM beam is collected and analyzed. Both angular and radial aperture configurations have been studied, demonstrating that even incomplete beam capture can provide mode-dependent intensity or phase signatures sufficient for reliable OAM mode identification without requiring full-beam collection [92]. Nevertheless, these methods have generally not been optimized to minimize bit error rate (BER) under realistic inter-satellite link conditions, where misalignment and noise strongly impact system performance.

Our recent work [15] addresses this gap by establishing a mathematical framework to determine the optimal photo-receiver location for binary OAM communication systems, thereby ensuring minimal BER. The model explicitly incorporates the effects of pointing error jitters, a critical impairment in satellite communication links arising from platform vibrations and tracking instabilities. Theoretical predictions were supported by simulation studies and further validated through laboratory experiments, with strong agreement observed between analytical and experimental results. This demonstrates that localized beam sampling can reliably decode OAM modes while reducing hardware complexity. Unlike prior studies that primarily provided proof-of-concept demonstrations, our contribution delivers a systematic and optimized detection strategy, positioning partial-beam reception as a practical and scalable solution for OAM-based free– space optical communication.

14.3 Summary and future perspectives

Our work introduced a sampled-beam detection strategy for orbital angular momentum (OAM) communication, aimed at addressing the fundamental limitation posed by beam divergence in long-range optical links. By analyzing only a localized portion of the received OAM beam, the approach avoids the need for full-beam capture and significantly reduces receiver aperture requirements. Through a rigorous mathematical framework, the study identified the optimal receiver position that minimizes the bit error rate (BER) in both perfectly aligned and misaligned scenarios. Importantly, the model accounted for pointing error jitters, which are inherent in practical satellite platforms, thereby enhancing the robustness of the scheme. The theoretical results were supported by simulations and further validated through experimental demonstrations, confirming that localized sampling can reliably decode OAM modes while maintaining low BER. This establishes the proposed method as a practical and efficient pathway for implementing OAM-based communication in inter-satellite links.

Looking forward, several promising directions emerge from this foundation. One immediate extension is to generalize the sampled-beam approach beyond binary OAM communication to multi-level and multiplexed systems, thereby unlocking higher spectral efficiency and throughput. Another important avenue is to investigate the role of wavelength scaling, since OAM beam divergence varies with wavelength, and hybrid schemes combining wavelength and OAM multiplexing may offer significant capacity gains. The detection of OAM states with equal magnitude but opposite signs, such as $\pm l$ modes, represents another open challenge that could further expand the encoding space and resilience of OAM communication. Beyond these physical-layer considerations, the integration of localized OAM detection into compact photonic integrated circuits (PICs) could accelerate practical deployment by enabling chip-scale receivers with reduced bulk and improved stability. Moreover, while the current work focused on inter-satellite communication where atmospheric effects are negligible, extending the framework to terrestrial free– space optical links will require careful consideration of turbulence and scattering. Finally, system-level prototyping in real satellite communication scenarios will be a crucial step toward validating scalability and link budget improvements under operational conditions.

In summary, the sampled-beam detection technique presented here lays the groundwork for future OAM-based communication systems that are more compact, resilient, and scalable. By combining theoretical modeling, experimental validation, and clear directions for future development, this research provides a pathway toward realizing next-generation free– space optical networks capable of supporting the growing demands of global connectivity.

15 Toward high-dimensional optical communication: deep learning for orbital angular momentum beams (Gokul Manavalan, Ganesh M Balasubramaniam and Shlomi Arnon)

15.1 Background

The search for ever-higher capacity in optical communication has historically revolved around exploiting new physical degrees of freedom (DoFs). Polarization,

wavelength-division multiplexing, and spatial multiplexing have each expanded system throughput. Orbital angular momentum (OAM) of light, characterized by vortex beams with helical phase singularities, represents the latest step in this evolution [11, 13]. Unlike conventional Gaussian beams, OAM beams provide access to an effectively unbounded state space defined by their topological charge, thereby enabling high-dimensional encoding and multiplexing in both classical and quantum regimes [14].

The key advantage of OAM beams lies in their orthogonality and modal diversity, which allow multiple independent data channels to coexist within the same spatial aperture. This property has motivated their use in free–space optical (FSO) or optical wireless communication (OWC), high-capacity wireless systems, and secure quantum key distribution [11]. However, translating this theoretical promise into practice is far from trivial. The propagation of OAM beams through realistic channels is susceptible to atmospheric turbulence, scattering, and absorption, which induce intensity scintillation, wavefront aberrations, and modal crosstalk. These impairments complicate reliable detection and significantly degrade system performance [14].

Willner et al. [11] framed OAM as part of a broader roadmap toward structured-light communications, covering multiplexing architectures, classical and quantum links, and technical hurdles such as turbulence and modal coupling in fibers. Their perspective positioned OAM as a powerful but transitional DoF—one that opens high-dimensional encoding possibilities but also demands co-development of mitigation strategies, from adaptive optics to advanced signal processing. Importantly, this sets the stage for artificial intelligence (AI) and deep learning to act not merely as auxiliary tools, but as core enablers of OAM-based communication. A general schematic illustrating the propagation and deep learning–based recovery of OAM beams is shown in Fig. 14.

15.2 Current state-of-the-art

The integration of deep learning with OAM communications marks a pivotal development in overcoming channel impairments. Conventional digital signal processing approaches—adaptive optics or MIMO equalization—struggle with scalability when channel conditions fluctuate rapidly or when multiple OAM modes are multiplexed. In contrast, deep learning (DL) models can directly learn mappings from distorted field patterns to mode labels or even to reconstructed fields, providing resilience under diverse and dynamic conditions [14, 93, 94].

Hongping Zhou et al. [93] advanced this direction by designing a ShuffleNet V2–based CNN for OAM mode recognition in turbulent free– space channels. Their model, trained on Laguerre–Gaussian intensity images, achieved accuracies as high as 99.5% for multiplexed OAM modes even under strong turbulence. Crucially, the trained network generalized well to turbulence intensities outside the training set, a property often missing in earlier works. This result illustrates that carefully designed DL architectures can not only achieve high precision but also robustness to environmental variability—an essential step toward real-world deployment.

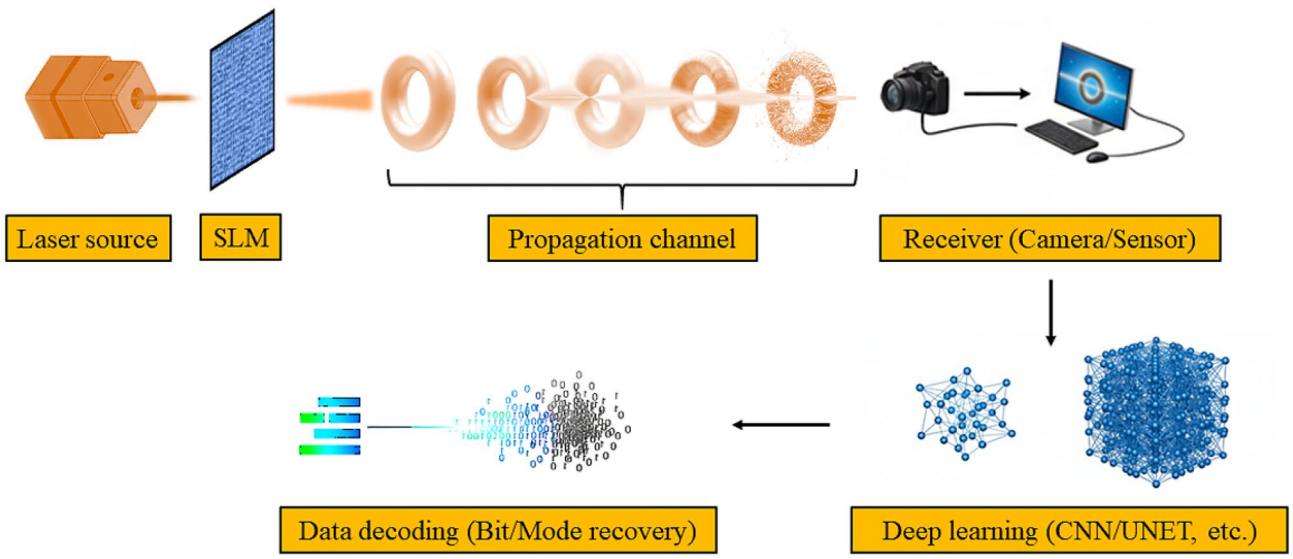

Fig. 14 General schematic of an OAM communication system integrated with deep learning. Structured beams generated via a spatial light modulator propagate through turbulence or scattering media. At the receiver, distorted intensity distributions are processed using deep learning models (e.g., CNNs, U-Net, transfer learning) for robust mode recognition and data recovery. The workflow highlights the synergy between structured light physics and AI for next-generation optical communication

Manavalan et al. [14] approached the problem from a complementary angle by embedding physical insight into the learning pipeline. Instead of directly classifying OAM modes, they employed the Conjugate Light Field (CLF) method, reducing the task to distinguishing between two CLF outputs. This reduction dramatically decreased the computational burden without compromising performance. In tabletop experiments, the system achieved a bit error rate (BER) of 2.44×10^{-4}, representing nearly a 99% reduction compared to baseline methods. The study demonstrated that physics informed deep learning not only boosts efficiency but also accelerates real time applicability, which is a crucial requirement for practical OWC systems.

The importance of beam selection further emerges when moving beyond Laguerre–Gaussian beams. In another study, Manavalan et al. [94] systematically compared Bessel–Gaussian (BG) and Ince–Gaussian (IG) beams for free– space links up to 500 m. BG beams, due to their non-diffracting and self-healing nature, exhibited superior robustness against distortions, outperforming IG beams whose asymmetric intensity patterns proved more vulnerable. Coupling this with DenseNet-201 and InceptionV3 architectures enabled accurate mode classification even under challenging propagation scenarios. This work illustrates a broader point: the performance of DL-based OAM communication is not only determined by the network but also by the physical choice of beam family.

Taken together, these results highlight a clear trajectory. Zhou et al. [93] demonstrated the strength of architecture optimization, while Manavalan et al. [14, 94] emphasized the synergy of physics-driven simplification and structured beam selection. The field is thus moving toward a dual strategy: leveraging DL's capacity for feature extraction while embedding physics to ensure scalability, interpretability, and efficiency.

15.3 Conclusions and future perspectives

The convergence of structured light and deep learning has already reshaped the landscape of OAM based communications. Demonstrations of turbulence compensation, multiplexed mode recognition, and physics informed learning pipelines have significantly expanded the feasibility of deploying OAM in real world links. Nevertheless, several challenges remain unresolved.

- Scalability of training, as OAM channel dimensionality increases, the volume of required training data grows exponentially.
- Residual turbulence effects, higher order OAM modes remain disproportionately sensitive to phase aberrations.
- Computational demands, training and inference on high resolution datasets impose non trivial hardware constraints.

Overcoming these limitations will likely require hybrid strategies

(i) Physics informed deep learning architectures that exploit beam symmetries.
(ii) Transfer learning and domain adaptation to reduce training costs.
(iii) Hybrid quantum classical neural networks to further accelerate pattern recognition.

In addition, structured beams such as Bessel Gaussian and Ince Gaussian families may complement or even outperform Laguerre Gaussian modes in certain environments, thereby broadening the toolkit for high dimensional encoding.

At the same time, a critical perspective is necessary. Kahn et al. [95] argued that OAM multiplexing does not fundamentally increase the capacity limits of free–space channels, as it is outperformed by multiplexing in complete modal bases or parallel Gaussian beams. They emphasize that OAM is not a new degree of freedom but a subset of the Laguerre–Gaussian family. This critique tempers overoptimistic claims, suggesting that OAM's role is less about surpassing Shannon capacity limits and more about enabling structured encoding, experimental versatility, and integration with AI-driven recovery.

Thus, the roadmap ahead for OAM-based communication should be viewed as twofold. On one side, deep learning will continue to unlock practical robustness, enabling FSO and OWC systems to operate under turbulent, long-distance conditions. On the other side, capacity scaling may ultimately require moving beyond OAM alone—toward full modal multiplexing strategies, hybrid beam families, and AI-driven channel-adaptive architectures. The synergy of physics and machine learning will remain the cornerstone of this transition, ensuring that OAM beams, while not a panacea, serve as a critical stepping stone toward truly high-dimensional optical communication.

16 Singular optics for coded aperture imaging (Narmada Joshi, Eulàlia Puig Vilardell, Francis Gracy Arockiaraj, Agnes Pristy Ignatius Xavier, Shivasubramanian Gopinath, Kaupo Kukli, Aile Tamm, Joseph Rosen, Darius Gailevičius, Saulius Juodkazis, and Vijayakumar Anand)

16.1 Background

Coded aperture imaging (CAI) is an indirect imaging technique that replaces traditional lenses with specially designed coded masks (CMs). Rather than recording a direct image of the object, these CMs encode incoming light from an object into structured patterns on a detector plane, from which computational reconstruction retrieves the object information. Compared with conventional imaging systems, CAI provides greater flexibility and has proven particularly powerful for advanced imaging applications [96]. A major milestone in the evolution of CAI is the development of interferenceless coded aperture correlation holography (I-COACH). In I-COACH, three independent response intensities to an object (RIOs) are recorded under incoherent illumination without two-beam interference using three different CMs. These RIOs are then projected into the complex domain by applying distinct phase shifts and then superposed to obtain the complex-valued hologram of the object. The object image is retrieved by cross-correlating the complex-valued hologram of the object with a precalibrated database of complex-valued holograms of the point object at different depths. Later, I-COACH was advanced to a single-camera-shot technique by introducing a new computational reconstruction algorithm, nonlinear reconstruction (NLR) [96, 97]. This simple yet powerful configuration enables single-shot 3D imaging and provides a flexible platform for extending CAI into multidimensional domains. In this chapter, we present I-COACH as a generalized framework for diverse imaging applications, employing the Lucy-Richardson-Rosen algorithm (LRRA) for image reconstruction [98–100]. We first describe how the method extends beyond random CMs to incorporate deterministic optical fields such as spiral lenses, spiral axicons, etc., transferring their unique propagation characteristics into imaging applications by a single camera shot [98]. We then highlight how specially designed modulation schemes, such as vortex ensemble generators (VEGs), enrich the encoding process by introducing orbital angular momentum (OAM) content into speckle ensembles [99]. Finally, we outline the extension of I-COACH to five-dimensional (5D) imaging, where spatial, spectral, and polarization information are encoded simultaneously [100]. Together, these advances establish I-COACH as a versatile platform unifying structured light beams and multidimensional imaging under a single incoherent imaging paradigm.

16.2 Methodology and results

The optical configuration of the I-COACH system is illustrated in Fig. 15a and b. The light emitted from an object is modulated by a CM, and the resulting RIO is recorded by an image sensor. A point spread function (PSF) library is pre-recorded at different depths, wavelengths, and polarization orientations and used as the reconstruction function. The object image is computationally retrieved by correlating the RIO with the corresponding PSFs using the LRRA.

Early implementations of I COACH primarily employed quasi random CMs. Recently, its applicability has been extended to deterministic optical fields, such as spiral lenses and spiral axicons [98]. These structured beams exhibit distinctive three dimensional propagation characteristics, such as nondiffracting and self healing behavior, but they lack a conventional point focus and are therefore unsuitable for direct imaging. By tailoring the CM design and applying LRRA based reconstruction, I COACH successfully transfers the exotic propagation signatures of these beams into imaging applications in a single shot. To further enrich the encoding process, VEGs have been introduced [99]. In VEG, random spiral phases with a wide range of topological charges are combined with linear phase components to control the propagation direction. The resulting ensembles of vortex beams interfere to produce chaotic yet highly structured speckle patterns that carry OAM. The sensor records these patterns, and the object image is reconstructed using the prerecorded PSF library via LRRA. Expanding this framework, five dimensional I COACH was recently demonstrated to capture spatial, spectral, and polarization information simultaneously in a single shot [100]. A composite optical modulator, consisting of a phase only, polarization sensitive spiral phase mask projected onto an amplitude only, polarization insensitive quasi random diffractive lens, generates unique RIOs corresponding to variations in depth, wavelength, and polarization. These RIOs are captured by an image sensor, and the complete multidimensional object information is retrieved computationally via LRRA using the PSF library without requiring multiple exposures or a polarization sensitive image sensor. The experimental results are summarized in Fig. 15c and d. Figure 15c shows the CMs, PSFs, RIOs, and reconstruction results via LRRA for deterministic optical fields in rows one and two and VEGs with $n = 4$

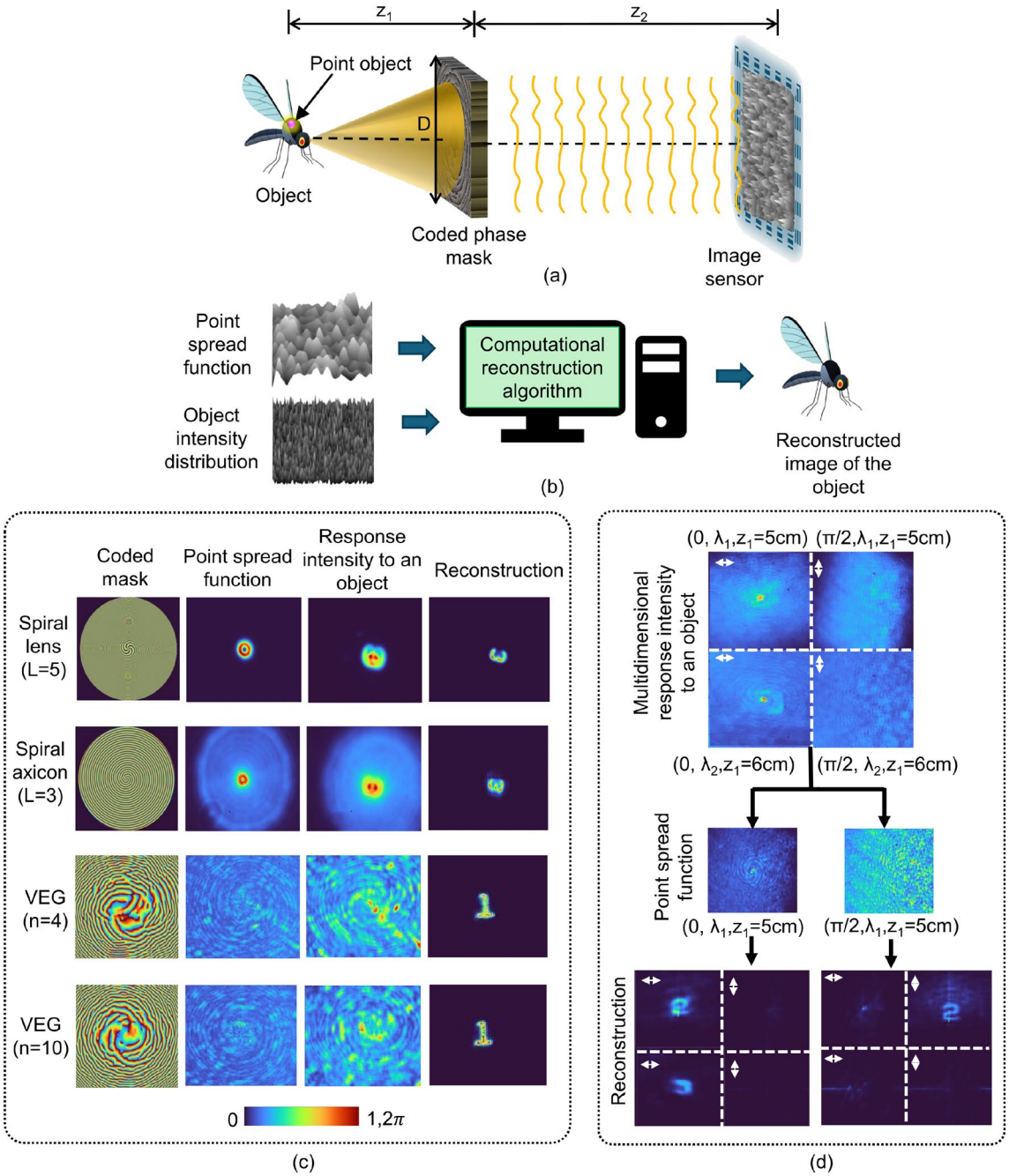

Fig. 15 Optical configuration of I COACH **a** Recording and **b** reconstruction process. Experimental results **c** CMs, PSFs, RIOs, and reconstruction results by LRRA of the spiral lens $(L = 5)$, spiral axicon $(L = 3)$, VEG $(n = 4)$, and VEG $(n = 10)$. The variables L and n indicate the topological charge and number of spiral phase elements, respectively. **d** 5D imaging across 3D space, spectrum, and polarization. Top multidimensional RIO corresponding to two depths $(z_1 = 5\ \text{cm}, z_2 = 6\ \text{cm})$, two polarization states $(0, \pi/2)$, and two wavelengths $(\lambda_1 = 660\ \text{nm}, \lambda_2 = 532\ \text{nm})$; Middle PSFs; Bottom reconstruction results by LRRA

and $n = 10$ in rows three and four. Figure 15d presents the five dimensional imaging results, including the multidimensional RIO, PSF, and reconstruction result via LRRA. The ranges of the reconstruction parameters, such as the number of iterations, α, and β, used in LRRA are from 5 to 70, from 0 to 0.8, and equal to 1, respectively.

16.3 Conclusions and future perspectives

In conclusion, I-COACH provides a unified framework for multidimensional incoherent imaging, evolving from quasirandom masks to deterministic optical fields, VEGs, and 5D imaging. Its ability to encode spatial, spectral,

and polarization information into a single framework highlights its versatility and potential for compact, high-performance imaging systems. Future directions include expanding to six-dimensional (6D) imaging by incorporating time, enabling real-time acquisition of dynamic multidimensional scenes, and offering a versatile platform for advanced optical imaging.

17 Probing Randomness with Topologically Structured Light (Cade Peters, Kelsey Everts and Andrew Forbes)

17.1 Background

As detailed in this roadmap, the field of singular optics has a long history, dating back more than half a century to the original work on dislocations in wave trains [1]. Over the past 30 years the field grew in the context of orbital angular momentum (OAM) [7] and structured light [6], recently experiencing a new surge of interest as the backbone on which to build topological light [101]. The interest here is to find states of structured light that are distortion-free, particularly through complex random media [102], which is known to be highly distorting and often requiring active compensation techniques. Topological light has been demonstrated to be promising in complex media, for instance, knots in turbulence [103], phase vortices in scattering media [104], and non-separability of vectorial light in unitary complex media [105], with growing evidence that topology is preserved in a variety of map preserving channels [106]. Here we probe random media with 1D and 2D forms of topological light and report the comparative performance. We use the tests to highlight the notion of new invariance that may be derived from structured light based on singular optics.

17.2 Methodology

To illustrate the notion of topologies and their comparative advantage, we consider three types of topologies, namely (i) scalar light fields with phase singularities that map phase to a wrapping around a circle, for one dimensional topology maps, (ii) vectorial fields with polarisation singularities, where the orientation and/or ellipticity of the polarisation ellipses is used to define a one dimensional map of the polarisation to a unit circle, and (iii) vectorial light with every polarisation embedded N times, for a two dimensional topology that wraps the Poincaré sphere N times over. These maps are illustrated in Fig. 16a. The question is whether all topologies are equal or whether some are more equal than others.

To systematically probe this question, we introduce the methodology of digital random media illustrated in Fig. 16b. We implement this as random realisations of binary phase masks encoded onto a spatial light modulator (SLM). These consist of square blocks with side length L each imparting 0 or π phase onto the input beam. Smaller blocks produce more rapidly varying phase distortions and thus choosing L relative to the beam diameter d tunes the distortion strength $\Omega = d/L$. This digitally imparts random phase fluctuations across the beam profile, simulating the action of a real world medium with stochastic refractive index fluctuations and an equivalent characteristic transverse correlation length L. We use similar digital technology to create the topological light, using a general vector beam creator that in special cases can be reduced to producing scalar phase vortices. Stokes projections and polarisation interferometry were used to extract the topological features of the light both before and after the medium.

17.3 Results

To demonstrate how this approach can be used for probing randomness, we use test cases of weak and strong scattering and show how the topological wrapping numbers can either change or remain invariant under the action of a complex medium. Results for phase singularities, polarisation singularities and optical skyrmions are shown in Fig. 16c for distortion strengths ranging from $\Omega = 1$ to $\Omega = 7$ and for three distinct wrapping numbers for each topology type. Each datapoint represents the average over 100 random realisations. We observe that although all three structures are fundamentally topological, they each behave differently under the action of the same perturbation. Phase singularities show a noticeable change in the wrapping number ℓ even at mild perturbation strengths Ω and a strong decay as Ω increases. In contrast, polarisation singularities exhibit superior robustness with small deviations from the encoded value m seen only for the largest wrapping number. Optical skyrmions show almost perfect invariance, with virtually no change in the wrapping number N as Ω increases.

It is reasonable to conclude that because the perturbation was phase-only, it had the largest effect on the topology constructed solely from phase. Polarisation singularities mix phase with a second degree of freedom (DoF), adding some additional resilience against the medium. Skyrmions are even further removed, combining phase, amplitude and polarisation to create a higher dimensional topology that is virtually immune to the effects of this channel. However, it is unknown if more complex channels or media that interact with other DoFs

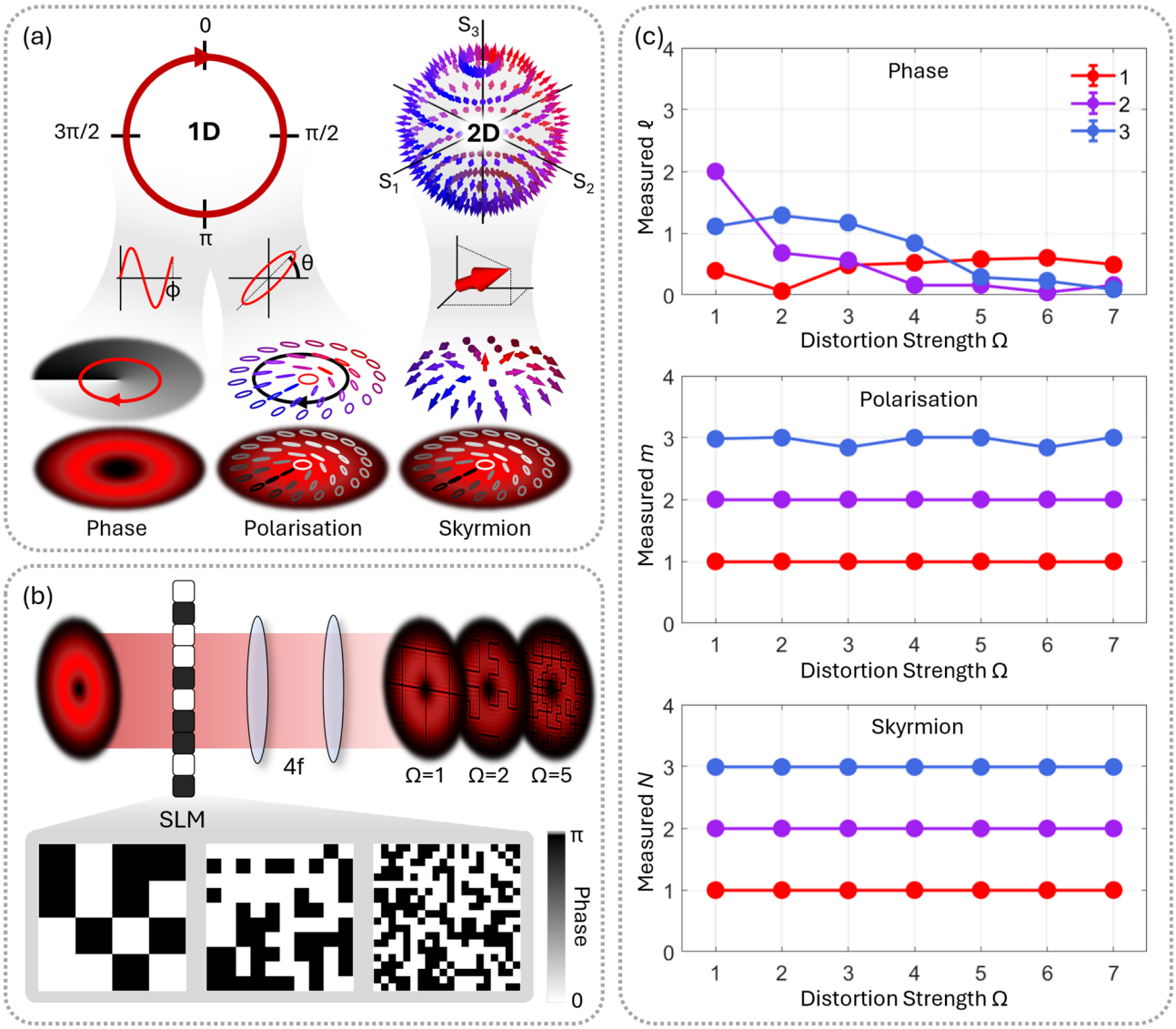

Fig. 16 **a** We consider three distinct topologies, namely phase singularities characterised by a point of undefined phase in a scalar complex field, polarisation singularities constructed from points of undefined orientation or ellipticity, and optical skyrmions which wrap the Poincaré sphere an integer number of times. **b** We digitally simulate a random scattering medium with the use of an SLM that imparts a spatially varying random binary phase onto an incident beam. The strength of the distortion Ω is controlled by varying how rapidly the imparted phase varies between 0 and π. **c** Plots showing the average measured wrapping number for each topology type as a function of Ω. We show three different wrapping numbers for each topology type and each datapoint represents the average over 100 random realisations

could show completely different results. The unique interactions between light's various DoFs provide a plethora of opportunities to explore and exploit the complex dynamics between topological light and the media through which it propagates.

17.4 Conclusions and future perspectives

Optical topologies have no natural energy barrier, yet their immutability can be guaranteed if the channel is map preserving. The promised benefit is robustness, which may be exploited for imaging and communication. Which channels are true to this remains an open question. Alas, detectors for topological light do not exist, an exciting open challenge that urgently requires addressing. Finally, complex media has historically been viewed as an obstacle to fully harnessing the potential of structured light, but a new take is to embrace complexity for optical computing [107]. Here, the movement and fragility of higher-order vortices may yet prove valuable by allowing nature to perform certain complex calculations at the speed of light. Additionally, disorder and distortion hold substantial information about the channel itself,

presenting the possibility of using fragile topologies for sensing and probing the useful properties of a medium.

18 Material manipulation using structured light beams (Takashige Omatsu and Srinivasa Rao Allam)

18.1 Background

Spatial control of laser beams is a topic garnering significant interest in the field of singular optics, and it enables the generation of versatile structured light beams, such as optical vortices, non-diffractive beams, and vector vortices.

In particular, optical vortices possess unique features including an annular spatial form with a dark central core (on-axis phase singularity) and orbital angular momentum (OAM). These characteristics are a function of the helical wavefront (helicity) of these laser beams, and they carry a so-called 'handedness' which is determined by the direction in which their helical wavefront twists. As such, these beams have the capacity to manipulate materials/media in exotic and unique ways.

For instance, chiral objects, which cannot be superposed onto their mirror image, exhibit the same physical properties as their mirror image; however, they show different optical absorption characteristics for left-handed or right-handed circularly polarized light. This property is known as circular dichroism and is a universal figure-of-merit used to describe the chirality of objects in materials science. Beyond conventional circular dichroism, optical vortex light–matter interactions via multipole transitions offer 'vortex dichroism' as a new figure of merit which can be used to describe higher-order structures of chiral engineered objects and metasurfaces [108].

Also, it has been discovered that optical vortices can twist irradiated materials, such as metals, semiconductors, and polymers, in clockwise (right-handed) or counterclockwise (left-handed) directions. This can be used to fabricate helical (chiral) structures on the nano/micro-scale; this approach can be used for the development of new chiral metasurfaces. Furthermore, optical vortices have demonstrated enantioselective control in chiral crystallization, in which an achiral crystal (or racemic compound) is twisted by OAM of irradiated optical vortices towards the clockwise or counterclockwise direction, thus yielding enantioselective polymorphic transformation into a *d* or *l*-chiral crystal. This demonstration offers new fundamental insights into the origin of homochirality [17, 19].

A non-contact direct printing technology enables the on-demand development of electronics, photonics, and biomedical devices with cost, energy, and resource savings. Optical vortex beams can be used to induce forward transfer/projection of materials. Here, the OAM of an optical vortex twists the irradiated donor material to produce the ejection of a spinning donor droplet with a perfectly straight flight path for the direct print of donor materials with a high spatial resolution at an extremely long working distance.

Structured light beams also include particle-like light waves known as optical quasiparticles. These include skyrmions, bimerons, and hopfions, all of which can manifest in two- or three-dimensional real space [109]. These optical quasiparticles are optical analogs of quasiparticles with topological spin textures which are encountered in solid-state physics. They carry topologically protected, space-invariant wavefront or polarization (lemon- or star-shaped) textures, even under the influence of perturbations, instead of spin textures. One of the most promising applications of such waves is thus in free– space communications under turbulent conditions. Also, they enable the manipulation of materials (creation and annihilation of exotic structures) and the ability to directly imprint topological structures onto condensed matter [110]. They further have the potential to revolutionize laser fabrication with submicron scaled ripple structures and polarization microscopy with high spatial resolution which exceeds the diffraction limit.

18.2 conclusions and future Perspectives

Structured light beams will facilitate interdisciplinary research across the fields of optics, physics, chemistry, mathematics, and life science, and they will enable the fabrication of nano- or micron-scale engineered structures with exotic physical properties (chirality, morphology and topology) unseen in natural materials owing to their strong SAM-OAM coupling effects.

Advancements in materials science hinges upon the development of novel structured light sources; however, compact structured light sources with both wavelength versatility and OAM tunability on a nano or submicron-scale are still in their infancy as a research topic and this needs to change. For instance, ultraviolet (UV) structured light sources will be applied in photochemical processes and nano/micro-fabrication, and extreme and deep UV structured light sources will be used to further explore advanced high-field and plasma physics. Furthermore, mid-infrared structured light sources will enable the development of super-resolution molecular spectroscopy with spatial resolution which exceeds the diffraction limit (Fig. 17).

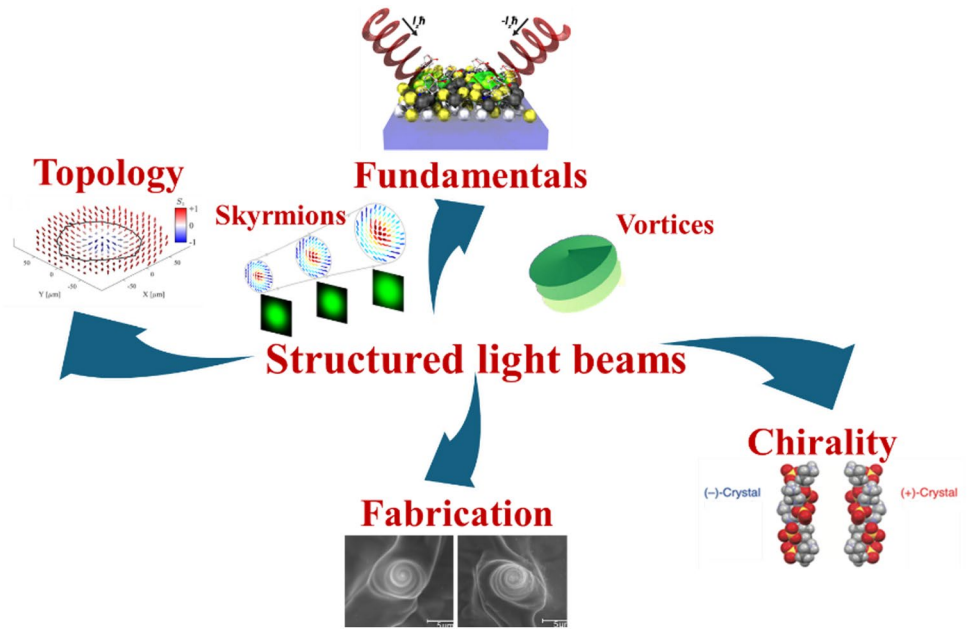

Fig. 17 Materials science with structured light beams [17, 108, 110]

19 High-harmonic generation with vortex laser fields (Andra Naresh Kumar Reddy)

19.1 Background

Higher-order harmonic generation (HHG) is a powerful nonlinear process in which ultrashort infrared pulses interact with gas or solid targets, producing coherent radiation as short as attoseconds over a range of timescales [111]. In the HHG process, precise control of the driving laser fields strongly dictates the spatial and spectral characteristics of the high-order harmonics [112–115]. In this context, a variety of driving laser fields created by modifying the spatial, temporal, and polarization properties of Gaussian beams are important in advancing light science [112–115]. With helically twisted wavefronts that carry orbital angular momentum, vortex laser fields have proven promising for driving the HHG process in gases [112–115].

19.2 Methodology and results

The experimental layout for generating high-harmonic vortex beams is shown in Fig. 18a. The Ti:sapphire laser emits infrared pulses with 60-fs duration, $\lambda = 800$ nm, and 500 μJ pulse energy, focused using a 500 mm lens. To produce vortex laser pulses with a topological charge $l = 1$, a spiral phase plate was utilized, imparting a linearly polarized, helical wavefront to the beam. Details on fabricating the spiral phase plate for creating vortex laser fields that drive high-order harmonic generation in gas are addressed in references [113, 114]. In the experiment (Fig. 18a), the vortex pump beam is focused onto an argon (Ar) gas jet inside a vacuum chamber, where it interacts with the gas as a single-color laser emission at 800 nm. Furthermore, higher-order harmonic beams, along with the fundamental beam, are directed towards the XUV spectrometer, where a variable line– space flat-field grating (FFG) disperses the resultant laser spectrum onto the micro-channel plate (MCP) combined with a phosphor screen. A charge-coupled device (CCD) camera captured images of the harmonic spectra from the phosphor screen of the MCP, as shown in Figs. 18c and d [113, 114]. During high nonlinear interaction with the Ar gas jet, the single-color driving field behavior is identical in the positive and negative half-cycles, resulting in symmetrical interaction that triggers the generation of odd harmonics, and the contribution of even harmonics is completely suppressed [111]. These odd harmonics exhibit double-lobe intensity profiles, separated by a dark region, which indicates a phase singularity or orbital angular momentum (OAM). The number of dark stripes observed across the harmonic beam corresponds to the topological charge conveyed by the harmonic beams [115]. The dark stripe orientation indicates the sign of the topological charge (l) that the higher-harmonic beam preserved [115]. The transverse intensity distribution of the vortex-driving beam is shown in Fig. 18b, while the odd harmonics with double-lobe intensity distributions are shown in Fig. 18c. The slanting direction of the dark areas is located midway between the harmonic beam intensity distributions marked in blue, as shown in Fig. 18c. Consequently, the sign and magnitude of the topological charge of odd-harmonics (H9, H11, H13, H15) with double-lobe intensity patterns are evaluated as a positive integer $(l = 1)$. However, the XUV Hartmann sensor coupled with CCD, in conjunction with the XUV

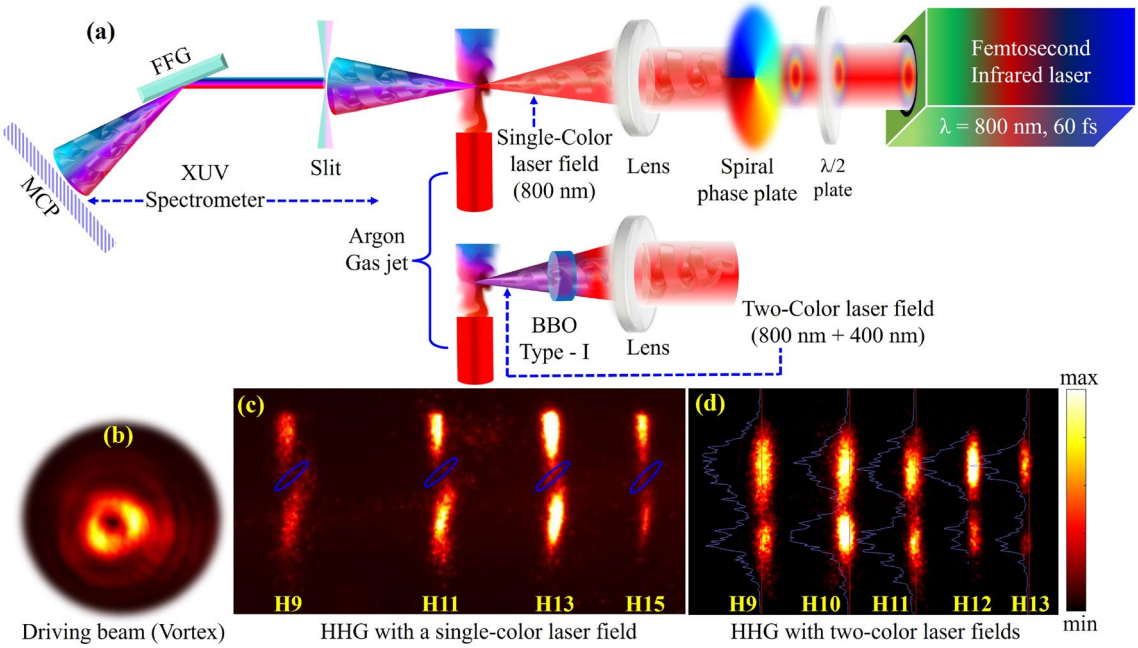

Fig. 18 **a** The experimental arrangement for HHG **b** driving vortex beam intensity profile near focus, HHG using **c** single-color, **d** two-color vortex laser fields [113, 114]

spectrometer, can be instrumental in precisely evaluating the wavefront or OAM of vortex beams.

To generate the HHG field containing both odd and even harmonics, inversion symmetry must be broken. This is achieved through the HHG process driven by two color laser fields. Consequently, a $0.2\ \mathrm{mm}$ thick barium borate (BBO) crystal was placed inside the vacuum chamber to produce second harmonic emission at $400\ \mathrm{nm}$, on the beam path of the focused single color laser or the fundamental beam $(800\ \mathrm{nm})$ before it interacts with the Ar gas jet.

During this nonlinear process, the second-harmonic conversion efficiency of the fundamental beam is approximately 5%. This creates a complex vortex-like intensity distribution $(\omega + 2\omega)$ at the focal spot, prompting a complex HHG field (H9 to H13), as shown in Fig. 18d. Note that the fundamental polarization is vertical, while the second-harmonic polarization is orthogonal, forming optimized orthogonal two-color laser fields [113, 114]. With this two-color pumping, even-order harmonics (H10, H12) become more prominent, and the $2(2n + 1)$ harmonic (H10) derived from the fundamental $(800\ \mathrm{nm})$ shows a strong intensity. The H10 is denoted as a fifth-order (odd) harmonic of the second-harmonic wave $(400\ \mathrm{nm})$. The odd and even vortex harmonic orders shown in Fig. 18d are polarized orthogonally, so H10 is polarized horizontally.

19.3 Conclusions and future perspectives

A two-color vortex laser field enables gentle control of the polarization directions of both odd and even harmonics simply by rotating the polarization of the fundamental radiation (800 nm), providing an elegant way to manipulate vortex harmonic light. In contrast, a single-color laser field produces odd-order harmonics with consistent orbital angular momentum. Generating extreme-ultraviolet vortex beams through HHG driven by single-color and two-color vortex laser fields is potentially useful in shaping attosecond pulses with orbital angular momentum and complex intensity patterns. Higher-order harmonic vortex beams are realized to yield beneficial results in XUV lithography, metrology, coherent diffractive imaging, and the control of molecular chirality and dichroism.

20 Summary and conclusions (Ganesh M. Balasubramaniam and Shlomi Arnon)

In this roadmap, singular optics is examined across its theoretical foundations, experimental methodologies, and emerging applications, with contributions that provide an overview of how optical singularities are understood, generated, and exploited. The chapters trace a progression from rigorous descriptions of phase, polarization, coherence, and spatiotemporal singularities, through strategies for tailoring and controlling these structures in propagation, to advanced

schemes for their measurement and use in complex photonic systems. This structure enables the reader to follow a coherent narrative from basic concepts to practical implementations in communication, imaging, material manipulation, and nonlinear and quantum photonics.

Collectively, the contributions confirm that singular optics has evolved from a largely theoretical topic into a mature framework that informs the design of sources, devices, and measurement architectures across many platforms. They demonstrate that topological features of optical fields can serve as robust resources for high dimensional information encoding, enhanced sensitivity in metrology and imaging, and tailored coupling to matter at the micro and nanoscale. At the same time, they expose common principles that recur across apparently different settings, such as the role of topological charge conservation, the interplay between spin and orbital degrees of freedom, and the use of mode and correlation measurements to reveal hidden structure in complex fields.

The assembled contributions also identify several pervasive challenges. One concerns the realization of scalable, low loss generation and detection of complex optical modes under realistic experimental constraints. Another arises in translating singular optics concepts into compact and robust photonic architectures that can operate reliably outside ideal laboratory conditions. A further challenge lies in developing theoretical and computational frameworks that treat partial coherence, temporal structure, and nonlinear interaction within a common description.

Future research in the fields of singular optics is expected to concentrate on the generation and control of increasingly complex optical fields, including higher order vortices with larger topological charges, hybrid phase–polarization singularities, and other multicomponent topological structures. The integration of singular optics with ultrafast photonics will enable the creation of spatiotemporal singularities in four dimensions (x, y, z, t), including optical pulses with temporal vortices, which opens new opportunities in nonlinear optics, attosecond science, and relativistic light–matter interactions. In parallel, a deeper understanding of singularities in nonparaxial and evanescent regimes, particularly in tightly focused fields or near material interfaces, will be essential for advances in nano optics and super resolution imaging.

Another major direction involves the integration of singular optics with emerging quantum and topological photonic platforms. Because optical singularities carry quantized topological charge, they provide natural high dimensional degrees of freedom for quantum information encoding, entanglement distribution, and the development of topologically protected quantum states. Embedding singularities into topological photonic crystals and non Hermitian systems is expected to yield new classes of defect immune optical modes guided jointly by field topology and photonic band topology.

Addressing real world complexity and enabling practical deployment are also central to future progress. Understanding how singularities propagate in scattering and disordered environments, including biological tissue, turbulent atmospheres, and multimode fibers, will drive the development of robust imaging, sensing, and communication technologies. At the same time, the miniaturization of singular optics systems through integrated photonics and metasurface based devices will support compact, manufacturable platforms such as vortex lasers, on chip singularity generators, and orbital angular momentum compatible photonic circuits. These capabilities are anticipated to underpin applications ranging from deep tissue imaging and advanced optical manipulation to precision materials processing.

Computational and machine learning driven methods will play a transformative role across all of these directions. Inverse design tools based on physics informed neural networks, differentiable Maxwell solvers, and evolutionary optimization can accelerate the discovery of complex singular fields and guide their engineering for specific propagation or interaction goals. Machine learning will also contribute to system level optimization by automating the generation, detection, and multiplexing of singular beams in communication and imaging platforms.

Progress on these fronts will benefit from closer interaction between communities that have often advanced in parallel, including those focused on wave theory, ultrafast science, quantum technologies, and device oriented engineering. By capturing the perspectives of many of the researchers who have driven these developments and by documenting representative recent advances, this roadmap is expected to serve as a reference point for current work, a guide to promising directions, and a stimulus for new collaborations that will shape the next stages in the evolution of singular optics.

Acknowledgements Chapters 6, 14 and 15: The authors express their gratitude to the Kreitman School of Advanced Graduate Studies and the Ben-Gurion University of the Negev for providing fellowships that supported our research endeavors. Chapter 18: ANKR conveys his sincere thanks to Rashid A. Ganeev from New Uzbekistan University and Helmut Zacharias from the University of Münster for providing resources.

Author contributions All authors contributed equally to the manuscript. The roadmap has been compiled by Ganesh M. Balasubramaniam.

Funding Chapter 3: MRF acknowledges funding from Singapore Ministry of Education Academic Research Fund (Tier 1) Grant Nos. RS13/23 and RG137/24. The authors acknowledge support from the DRDO grant no. DGTM/DFTM/GIA/24-25/426. Chapter 7: AHD

acknowledges funding from the Optica Foundation Challenge program and the Dutch Research Council (NWO) Vidi program, Chapter 8: The authors acknowledge the generous support from Airbus Institute for Engineering Research (AIER) and Office of Naval Research (N00014-20-1-2558, N00014-20-1-2789, N6833522C0344, and N6833523C0735), Chapter 10: The authors acknowledge financial support from the Czech Science Foundation (grant No. 25-17500 S), Chapter 12: SGR would like to acknowledge the support from ISRO through respond program (ISRO/RES/3/958/24-25). RK would like to acknowledge the support from the Anusandhan National Research Foundation (ANRF), Government of India, under the SERB SURE research grant (File No. SUR/2022/000910) and SRM University – AP for seed grants SRMAP/URG/SEED/2023-24/044 and SRMAP/URG/SEED/2024-25/041, Chapters 6, 14 and 15: The authors acknowledge the funding from the Israel Science Foundation (ISF) for the financial support of our project under grant number 897/21, Chapter 16: This research was funded by the European Union's Horizon 2020 research and innovation programme grant agreement No. 857627 (CIPHR), the Australian Research Council, Grant No. DP240103231, and the Israel Science Foundation (ISF) Grant No. 3306/25.

Data availability No datasets were generated or analysed during the current study.

Declarations

Conflict of interest The authors declare no conflict of interest.

References

1. J.F. Nye, M.V. Berry, Dislocations in wave trains. Proceed. Royal Soc. London A **336**, 165–190 (1974)
2. M.S. Soskin, M.V. Vasnetsov, Singular optics, in *Progress Opt.*, vol. 42, ed. by E. Wolf (Elsevier, Amsterdam, The Netherlands, 2001), pp.219–276
3. M.R. Dennis, K. O'Holleran, M.J. Padgett, Singular optics: optical vortices and polarization singularities. In: E. Wolf, (ed.) Progress in Optics. Progress in Optics, vol. 53, pp. 293–363. Elsevier, Amsterdam (2009). Chap. 5. https://doi.org/10.1016/S0079-6638(08)00205-9
4. Y. Yang, Y.-X. Ren, C. Rosales-Guzmán, Optical vortices: fundamentals and applications. IOP Series in Advances in Optics, Photonics and Optoelectronics, p. 240. IOP Publishing, Bristol, UK (2024). https://doi.org/10.1088/978-0-7503-5844-6
5. C. Rosales-Guzmán, B. Ndagano, A. Forbes, A review of complex vector light fields and their applications. J. Opt. **20**(12), 123001 (2018)
6. A. Forbes, M. Oliveira, M.R. Dennis, Structured light. Nat. Photonics **15**, 253–262 (2021)
7. A. Forbes, L. Mkhumbuza, L. Feng, Orbital angular momentum lasers. Nat. Rev. Phys. **6**, 352–364 (2024)
8. H. Rubinsztein-Dunlop, A. Forbes, M.V. Berry, M.R. Dennis, D.L. Andrews, M. Mansuripur, C. Denz, C. Alpmann, P. Banzer, T. Bauer, E. Karimi, L. Marrucci, M. Padgett, M. Ritsch-Marte, N.M. Litchinitser, N.P. Bigelow, C. Rosales-Guzmán, A. Belmonte, J.P. Torres, T.W. Neely, M. Baker, R. Gordon, A.B. Stilgoe, J. Romero, A.G. White, R. Fickler, A.E. Willner, G. Xie, B. McMorran, A.M. Weiner, Roadmap on structured light. J. Opt. **19**(1), 013001 (2017)
9. A.E. Willner, H. Zhou, X. Su, Perspective on tailoring longitudinal structured beam and its applications. Nanophotonics **14**(23), 3803–3812 (2025)
10. M.H. Ansari, V.M. Cris, R. Kumar, V. Anand, S. Prabhakar, S.G. Reddy, R.P. Singh, Scattering of open vortex beams: applications towards free space optical communications. Opt. Lasers Eng. **193**, 109090 (2025)
11. A.E. Willner, H. Song, K. Zou, H. Zhou, X. Su, Orbital angular momentum beams for high-capacity communications. J. Lightwave Technol. **41**(7), 1918–1933 (2023)
12. A.E. Willner, H. Huang, Y. Yan, Y. Ren, N. Ahmed, G. Xie, C. Bao, L. Li, Y. Cao, Z. Zhao et al., Optical communications using orbital angular momentum beams. Adv. Opt. Photon. **7**(1), 66–106 (2015)
13. G.M. Balasubramaniam, R. Kumar, S. Arnon, Vortex beams and deep learning for optical wireless communication through turbulent and diffuse media. J. Lightwave Technol. **42**(10), 3631–3641 (2024)
14. G. Manavalan, G.M. Balasubramaniam, S. Arnon, Improving oam-based optical wireless communication in turbulence using conjugate light field and hybrid neural networks. J. Lightwave Technol. **43**(7), 3211–3221 (2025)
15. A. Mehra, S. Arnon, Optimal receiver design for orbital angular momentum (OAM) communication via sampled beam analysis. J. Lightwave Technol. **43**(9), 4193–4202 (2025)
16. G.M. Balasubramaniam, N. Biton, S. Arnon, Imaging through diffuse media using multi-mode vortex beams and deep learning. Sci. Rep. **12**(1), 1561 (2022)
17. T. Omatsu, K. Miyamoto, K. Toyoda, R. Morita, Y. Arita, K. Dholakia, A new twist for materials science: the formation of chiral structures using the angular momentum of light. Adv. Opt. Mater. **7**(14), 1801672 (2019)
18. A.H. Dorrah, N.A. Rubin, A. Zaidi, M. Tamagnone, F. Capasso, Metasurface optics for on-demand polarization transformations along the optical path. Nat. Photonics **15**, 287–296 (2021)
19. K. Toyoda, H.-T. Su, K. Miyamoto, T. Sugiyama, T. Omatsu, Chiral crystallization manipulated by orbital angular momentum of light. Optica **10**(3), 332–338 (2023)
20. A.M. Yao, M.J. Padgett, Orbital angular momentum: origins, behavior and applications. Adv. Opt. Photonics. **3**(2), 161–204 (2011)
21. Y. Shen, X. Wang, Z. Xie, C. Min, X. Fu, Q. Liu, M. Gong, X. Yuan, Optical vortices 30 years on: OAM manipulation from topological charge to multiple singularities. Light: Science & Applications, 8 90 (2019)
22. M. Cheng, W. Jiang, L. Guo, J. Li, A. Forbes, Metrology with a twist: probing and sensing with vortex light. Light Sci. Appl. **14**(1), 4 (2025)
23. J.P. Torres, L. Torner, Twisted Photons: Applications of Light with Orbital Angular Momentum, p. 243. Wiley-VCH, Weinheim. (2011) https://doi.org/10.1002/9783527635368
24. X.-B. Hu, C.-X. Liu, Y.-C. Zhu, R.-P. Chen, B. Zhao, F.-M. Wu, C. Rosales-Guzmán, Inhomogeneous enantiomeric solution

concentration measurement harnessing vectorial structured light. ACS Photon. **11**(11), 4533–4540 (2024)
25. B. Ndagano, I. Nape, M.A. Cox, C. Rosales-Guzmán, A. Forbes, Creation and detection of vector vortex modes for classical and quantum communication. J. Lightwave Technol. **36**(2), 292–301 (2018)
26. M.R. Foreman, P. Török, Computational methods in vectorial imaging. J. Mod. Opt. **58**, 339–364 (2011)
27. C.J.R. Sheppard, S. Wales, P. Török, Efficient calculation of electromagnetic diffraction in optical systems using a multipole expansion. J. Mod. Opt. **44**, 803–818 (1997)
28. M.R. Foreman, Y. Sivan, S.A. Maier, P. Török, Independence of plasmonic near-field enhancements to illumination beam profile. Phys. Rev. B **86**(15), 155441 (2012)
29. M.R. Foreman, P. Török, Spin-orbit coupling and conservation of angular momentum flux in non-paraxial imaging of forbidden radiation. New J. Phys. **13**, 063041 (2011)
30. Palacios, D. M., Maleev, I. D., Marathay, A.S., & Swartzlander Jr, G. A. (2004). Spatial correlation singularity of a vortex field. Physical review letters, 92(14), 143905
31. R.K. Singh, A.M. Sharma, P. Senthilkumaran, Vortex array embedded in a partially coherent beam. Opt. Lett. **40**(12), 2751–2754 (2015)
32. A. Yadav, T. Sarkar, T. Suzuki, R.K. Singh, Detecting topological charge and phase of the vortex beam embedded into the low coherence background. Opt. Lasers Eng. **184**(1), 108668 (2025)
33. A. Gautam, A.K. Agarwal, R.K. Singh, Coherence vortices by binary pinholes. Nanophotonics **13**(24), 4397–4407 (2024)
34. R.K. Singh, D.N. Naik, H. Itou, M.M. Brundabanam, Y. Miyamoto, M. Takeda, Vectorial van Cittert-Zernike theorem based on spatial averaging: experimental demonstrations. Opt. Lett. **38**(22), 4809–4812 (2013)
35. S.A. Ponomarenko, A class of partially coherent beams carrying optical vortices. J. Opt. Soc. Am. A **18**(1), 150–156 (2001)
36. Z. Mei, O. Korotkova, D. Zhao, Y. Mao, Self-focusing vortex beams. Opt. Lett. **46**(10), 2384–2387 (2021)
37. Y. Zhang, Y. Cai, G. Gbur, Partially coherent vortex beams of arbitrary radial order and a an Cittert-Zernike theorem for vortices. Phys. Rev. A **101**, 043812 (2020)
38. W. Miao, Y. Zhang, G. Gbur, Deterministic vortices evolving from partially coherent fields. Optica **10**(9), 1173–1176 (2023)
39. R. Qi, G. Gbur, Deterministic vortex revivals in partially coherent beams. Opt. Lett. **50**(14), 4570–4573 (2025)
40. N. Jhajj, I. Larkin, E.W. Rosenthal, S. Zahedpour, J.K. Wahlstrand, H.M. Milchberg, Spatiotemporal optical vortices. Phys. Rev. X **6**, 031037 (2016)
41. S.W. Hancock, S. Zahedpour, A. Goffin, H.M. Milchberg, Free-space propagation of spatiotemporal optical vortices. Optica **6**(12), 1547–1553 (2019)
42. W. Chen, Y. Liu, Y.-Q. Lu, Spatiotemporal optical vortices: toward tailoring orbital angular momentum of light in full space-time. ACS Photonics **10**(7), 2011–2019 (2023)
43. N. Yu, F. Capasso, Flat optics with designer metasurfaces. Nat. Mater. **13**, 139–150 (2014)
44. T. Mayteevarunyoo, B.A. Malomed, D.V. Skryabin, Spatiotemporal dissipative solitons and vortices in a multi-transverse-mode fiber laser. Opt. Express **27**(26), 37364–37373 (2019)
45. A.H. Dorrah, M. Zamboni-Rached, M. Mojahedi, Controlling the topological charge of twisted light beams with propagation. Phys. Rev. A **93**(6), 063864 (2016)
46. L. Rego, K.M. Dorney, N.J. Brooks, Q.L. Nguyen, C.-T. Liao, J. San Román, D.E. Couch, A. Liu, E. Pisanty, M. Lewenstein, L. Plaja, H.C. Kapteyn, M.M. Murnane, C. Hernández-García, Generation of extreme-ultraviolet beams with time-varying orbital angular momentum. Science **364**(6447), 9486 (2019)
47. A.H. Dorrah, A. Palmieri, L. Li, F. Capasso, Rotatum of light. Sci. Adv. **11**(5), 9092 (2025)
48. A.H. Dorrah, N.A. Rubin, M. Tamagnone, A. Zaidi, F. Capasso, Structuring total angular momentum of light along the propagation direction with polarization-controlled meta-optics. Nat. Commun. **12**, 6249 (2021)
49. G. Sande, D. Brunner, M.C. Soriano, Advances in photonic reservoir computing. Nanophotonics **6**(3), 561–576 (2017)
50. L. Allen, M.W. Beijersbergen, R.J.C. Spreeuw, J.P. Woerdman, Orbital angular momentum of light and the transformation of Laguerre-Gaussian laser modes. Phys. Rev. A **45**(11), 8185–8189 (1992)
51. X. Su, K. Zou, H. Zhou, H. Song, Y. Wang, R. Zeng, Z. Jiang, Y. Duan, M. Karpov, T.J. Kippenberg, M. Tur, D.N. Christodoulides, A.E. Willner, Temporally and longitudinally tailored dynamic space-time wave packets. Opt. Express **32**(15), 26653–26666 (2024)
52. J.J. Gil, R. Ossikovski, *Polarized Light and the Mueller Matrix Approach* (CRC Press, Boca Raton, FL, USA, 2016)
53. O. Korotkova, Orbitalization ellipse of a light beam. Opt. Lett. **50**(2), 391–394 (2025)
54. O. Korotkova, Orbitalization structure of random light beams. J. Opt. **27**(6), 065606 (2025). https://doi.org/10.1088/2040-8986/addc7c
55. J. Laatikainen, O. Korotkova, On the structure of the polarization-orbitalization tensor. Opt. Lett. **50**(17), 5258–5261 (2025)
56. S. Brasselet, M.D. Lew, Single-molecule orientation and localization microscopy. Nat. Photonics **19**(9), 925–937 (2025)
57. N.S. Ginsberg, C.-L. Hsieh, P. Kukura, M. Piliarik, V. Sandoghdar, Interferometric scattering microscopy. Nat. Rev. Methods Primers **5**(1), 23 (2025)
58. L. Marrucci, C. Manzo, D. Paparo, Optical spin-to-orbital angular momentum conversion in inhomogeneous anisotropic media. Phys. Rev. Lett. **96**(16), 163905 (2006)
59. T. Fordey, P. Bouchal, P. Schovanek, M. Baranek, Z. Bouchal, P. Dvorak, M. Hrton, K. Rovenska, F. Ligmajer, R. Chmelik, T. Sikola, Single-shot three-dimensional orientation imaging of nanorods using spin to orbital angular momentum conversion. Nano Lett. **21**(17), 7244–7251 (2021)
60. P. Bouchal, P. Dvorak, M. Hrton, K. Rovenska, R. Chmelik, T. Sikola, Z. Bouchal, Single-shot aspect ratio and orientation imaging of nanoparticles. ACS Photonics **10**(9), 3331–3341 (2023)
61. A. Shikder, N.K. Nishchal, Generation of optical vortex lattices by in-line phase modulation with partially coherent light. J. Opt. Soc. Am. A **40**(6), 1231–1236 (2023)
62. M. Baliyan, N.K. Nishchal, Generating scalar and vector modes of bessel beams utilizing holographic axicon phase with spatial light modulator. J. Opt. **25**, 095702 (2023)
63. A. Shikder, J.B. Mohapatra, N.K. Nishchal, Fractional topological charge measurement through optical correlation. Opt. Lett. **49**(8), 2017–2020 (2024)
64. H. Zhang, J. Zeng, X. Lu, Z. Wang, C. Zhao, Y. Cai, Review on fractional vortex beam. Nanophotonics **11**(2), 241–273 (2022). https://doi.org/10.1515/nanoph-2021-0616
65. V.V. Kotlyar, A.A. Kovalev, A.G. Nalimov, A.P. Porfirev, Evolution of an optical vortex with an initial fractional topological charge. Phys. Rev. A **102**(2), 023516 (2020). https://doi.org/10.1103/PhysRevA.102.023516
66. A.J. Jesus-Silva, E.J.S. Fonseca, J.M. Hickmann, Study of the birth of a vortex at fraunhofer zone. Opt. Lett. **37**(21), 4552–4554 (2012). https://doi.org/10.1364/OL.37.004552
67. E. Peters, G. Funes, E. Tajahuerce, Non-integer tangential singular beams in the near field: collinear phase-shifting holography for topological charge determination. Chaos **35**(4), 043101 (2025). https://doi.org/10.1063/5.0258239

68. E. Peters, G. Funes, L. Martínez-León, E. Tajahuerce, Analysis of practical fractional vortex beams at far field. Opt. & Laser Technol. **156**, 108480 (2022). https://doi.org/10.1016/j.optlastec.2022.108480
69. R. Kumar, S.K. Rao, N.K. Nishchal, A. Alfalou, Determining topological charges of an optical vortex array using correlation filter. Opt. Laser Technol. **189**, 113069 (2025)
70. G. Molina-Terriza, J.P. Torres, L. Torner, Twisted photons. Nat. Phys. **3**(5), 305–310 (2007)
71. C. Hua, G.B. Halász, E. Dumitrescu, M. Brahlek, B. Lawrie, Optical vortex manipulation for topological quantum computation. Phys. Rev. B **104**(10), 104501 (2021)
72. M.H.M. Passos, M.R. Lemos, S.R. Almeida, W.F. Balthazar, L. Silva, J.A.O. Huguenin, Speckle patterns produced by an optical vortex and its application to surface roughness measurements. Appl. Opt. **56**(2), 330–335 (2017)
73. F. Khanom, N. Mohamed, I. Lopushenko, A. Sdobnov, A. Doronin, A. Bykov, E. Rafailov, I. Meglinski, Twists through turbidity: propagation of light carrying orbital angular momentum through a complex scattering medium. Sci. Rep. **14**, 20662 (2024)
74. J.W. Goodman, *Speckle Phenomena in Optics: Theory and Applications* (Roberts and Company Publishers, Englewood, CO, 2007), p.387
75. J.C. Ricklin, F.M. Davidson, Atmospheric turbulence effects on a partially coherent Gaussian beam: implications for free-space laser communication. J. Opt. Soc. Am. A **19**(9), 1794–1802 (2002)
76. P. Kumar, A. Fatima, N.K. Nishchal, Image encryption using phase-encoded exclusive-OR operations with incoherent illumination. J. Opt. **21**(6), 065701 (2019)
77. W. Heeman, K. Dijkstra, C. Hoff, S. Koopal, J.P. Pierie, H. Bouma, E.C. Boerma, Application of laser speckle contrast imaging in laparoscopic surgery. Biomed. Opt. Express **10**(4), 2010–2019 (2019)
78. A.F. Fercher, J.D. Briers, Flow visualization by means of single-exposure speckle photography. Opt. Commun. **37**(5), 326–330 (1981)
79. X. Li, Y. Tai, F. Lv, Z. Nie, Measuring the fractional topological charge of LG beams by using interference intensity analysis. Opt. Commun. **334**, 235–239 (2015)
80. G.C.G. Berkhout, M.W. Beijersbergen, Method for probing the orbital angular momentum of optical vortices in electromagnetic waves from astronomical objects. Phys. Rev. Lett. **101**, 100801 (2008)
81. J. Lu, C. Cao, Z. Zhu, B. Gu, Flexible measurement of high-order optical orbital angular momentum with a variable cylindrical lens pair. Appl. Phys. Lett. **116**(20), 201105 (2020)
82. H. Wang, Y. Liang, X. Zhang, S. Chen, L. Shen, L. Zhang, J. Luo, J. Wang, Low-loss orbital angular momentum ring-core fiber: design, fabrication and characterization. J. Lightwave Technol. **38**(22), 6327–6333 (2020)
83. S.G. Reddy, S. Prabhakar, A. Kumar, J. Banerji, R.P. Singh, Higher order optical vortices and formation of speckles. Opt. Lett. **39**(15), 4364–4367 (2014)
84. M.V. Cris, V. Patnala, S.G. Reddy, C.R. Alves, Correlation between coherent and scattered optical vortices: diagnosis of the topological charge. Appl. Phys. B **129**, 85 (2023)
85. V. Raskatla, P.S. Badavath, S. Patil, V. Kumar, R.P. Singh, Speckle-based deep learning approach for classification of orbital angular momentum modes. J. Opt. Soc. Am. A **39**(5), 759–766 (2022)
86. P.S. Badavath, V. Raskatla, T.P. Chakravarthy, V. Kumar, Speckle-based structured light shift-keying for non-line-of-sight optical communication. Appl. Opt. **62**(19), 53–60 (2023)
87. P.S. Badavath, V. Raskatla, V. Kumar, 1D speckle-learned structured light recognition. Opt. Lett. **49**(5), 1045–1048 (2024)
88. P.S. Badavath, V. Kumar, Single-pixel orbital angular momentum detection in the temporal domain. J. Opt. **27**(1), 01–01 (2025)
89. P.S. Badavath, V. Kumar, Mapping 2D spatial structured light information onto 1D temporal speckle sequence. J. Opt. Soc. Am. A **42**(8), 1425–1433 (2025)
90. M.J. Padgett, F.M. Miatto, M.P. Lavery, A. Zeilinger, R.W. Boyd, Divergence of an orbital-angular-momentum-carrying beam upon propagation. New J. Phys. **17**(2), 023011 (2015)
91. W.J. Kammerer III, Development of optical communication terminals for increasing connectivity on small satellites. PhD thesis, Massachusetts Institute of Technology (2024)
92. X. Zhong, Y. Zhao, G. Ren, S. He, Z. Wu, Influence of finite apertures on orthogonality and completeness of Laguerre-Gaussian beams. IEEE Access **6**, 8742–8754 (2018)
93. H. Zhou, Z. Pan, M.I. Dedo, Z. Guo, High-efficiency and high-precision identification of transmitting orbital angular momentum modes in atmospheric turbulence based on an improved convolutional neural network. J. Opt. **23**(6), 065701 (2021)
94. G. Manavalan, S. Arnon, Comparative analysis of Bessel-Gaussian and Ince-Gaussian beams for free-space optical communication. In: H. Hemmati, B.S. Robinson, (eds.) Free-Space Laser Communications XXXVII. Proceedings of SPIE, vol. 13355, pp. 133550. SPIE, San Francisco, CA, US (2025). https://doi.org/10.1117/12.3047861
95. J.M. Kahn, G. Li, X. Li, N. Zhao, Are OAM states an optimal basis for spatially multiplexed free-space links? In: 2016 IEEE Photonics Society Summer Topical Meeting Series (SUM), pp. 42–43 (2016)
96. J. Rosen, A. Vijayakumar, M. Kumar, M.R. Rai, R. Kelner, Y. Kashter, A. Bulbul, S. Mukherjee, Recent advances in self-interference incoherent digital holography. Adv. Opt. Photonics. **11**(1), 1–66 (2019)
97. M.R. Rai, A. Vijayakumar, J. Rosen, Non-linear adaptive three-dimensional imaging with interferenceless coded aperture correlation holography (I-COACH). Opt. Express **26**(14), 18143–18154 (2018)
98. A.P. Ignatius Xavier, F.G. Arockiaraj, S. Gopinath et al., Single-shot 3D incoherent imaging using deterministic and random optical fields with Lucy-Richardson-Rosen algorithm. Photonics **10**(11), 987 (2023)
99. E. Puig Vilardell, S. Gopinath, V. Tiwari et al., Spatio-spectral correlations in interferenceless coded aperture correlation holography with vortex speckles. Appl. Phys. B **131**(10), 142 (2025)
100. N. Joshi, V. Tiwari, T. Kahro et al., Interferenceless coded aperture correlation holography for five-dimensional imaging of 3D space, spectrum and polarization. J. Phys.: Photonics **7**(2), 025004 (2025)
101. Y. Shen, Q. Zhang, P. Shi, L. Du, X. Yuan, A.V. Zayats, Optical skyrmions and other topological quasiparticles of light. Nat. Photonics **18**, 15–25 (2024)
102. S. Gigan, O. Katz, H.B. De Aguiar, E.R. Andresen, A. Aubry, J. Bertolotti, E. Bossy, D. Bouchet, J. Brake, S. Brasselet, Y. Bromberg et al., Roadmap on wavefront shaping and deep imaging in complex media. J. Phys. Photonics **4**, 042501 (2022)
103. D.G. Pires, D. Tsvetkov, H. Barati Sedeh, N. Chandra, N.M. Litchinitser, Stability of optical knots in atmospheric turbulence. Nat. Commun. **16**, 3001 (2025)
104. I. Meglinski, I. Lopushenko, A. Sdobnov, A. Bykov, Phase preservation of orbital angular momentum of light in multiple scattering environment. Light: Sci. Appl. **13**, 214 (2024)
105. I. Nape, K. Singh, A. Klug, W. Buono, C. Rosales-Guzmán, A. McWilliam, S. Franke-Arnold, A. Forbes, Revealing the invariance of vectorial structured light in complex media. Nat. Photonics **16**, 538–546 (2022)
106. A.A. Wang, Z. Zhao, Y. Ma, Y. Cai, R. Zhang, X. Shang, Y. Zhang, J. Qin, Z.-K. Pong, T. Marozsák et al., Topological protection of

optical skyrmions through complex media. Light: Sci. Appl. **13**, 314 (2024)
107. Z. Zhang, L. Kong, L. Zhang, X. Pan, T. Das, B. Wang, B. Liu, F. Wang, I. Nape, Y. Shen, A. Forbes, Structured light meets machine intelligence. eLight **5**, 26 (2025)
108. W. Brullot, M.K. Vanbel, T. Swusten, T. Verbiest, Resolving enantiomers using the optical angular momentum of twisted light. Sci. Adv. **2**(4), 1501349 (2016)
109. S.R. Allam, Y. Yoneda, T. Omatsu, Optical quasiparticles in paraxial laser beams. Prog. Opt. **70**, 281–338 (2025)
110. C. Mitra, C.S. Madasu, L. Gabardos, C.C. Kwong, Y. Shen, J. Ruostekoski, D. Wilkowski, Topological optical skyrmion transfer to matter. APL Photonics **10**(4), 046113 (2025)
111. A. L'Huillier, Nobel lecture: the route to attosecond pulses. Rev. Mod. Phys. **96**(3), 030503 (2024)
112. R. Martín-Hernández, G. Gui, L. Plaja, H.K. Kapteyn, M.M. Murnane, C.-T. Liao, M.A. Porras, C. Hernández-García, Extreme-ultraviolet spatiotemporal vortices via high harmonic generation. Nat. Photonics **19**(8), 817–824 (2025)
113. V. Kärcher, V.V. Kim, A.N.K. Reddy, H. Zacharias, R.A. Ganeev, Generation of complex vector and vortex extreme ultraviolet beams using the s-waveplate and spiral phase plate during high-order harmonics generation in argon. ACS Photonics **10**(12), 4519–4528 (2023)
114. A.N.K. Reddy, V.V. Kim, V. Kärcher, H. Zacharias, A. Bundulis, A. Sarakovskis, A. Atvars, A. Ubelis, R.A. Ganeev, Spatial shaping of low- and high-order harmonics generated using vortex beams. J. Phys. D Appl. Phys. **57**(30), 305105 (2024)
115. Y. Hu, Z. Ye, H. Li, C. Lu, F. Chen, J. Wang, S. Pan, M. Zhang, J. Gao, J. Wu, Generation of vortex n2+ lasing. Optica **10**(6), 682–687 (2023)

Authors and Affiliations

Ganesh M. Balasubramaniam[1] · Srinivasa Rao Allam[2] · Vijayakumar Anand[3,4] · Md. Haider Ansari[5] · Francis Gracy Arockiaraj[3,6] · Shlomi Arnon[6] · Purnesh Singh Badavath[7] · Mansi Baliyan[21] · Petr Bouchal[8,9] · Zdeněk Bouchal[10] · Sakshi Choudhary[5] · Ahmed H. Dorrah[11] · Yuxiang Duan[12] · Kelsey Everts[13] · Andrew Forbes[13] · Matthew R. Foreman[1,14] · Darius Gailevičius[15] · Akanksha Gautam[16] · Greg Gbur[17] · Shivasubramanian Gopinath[3] · Narmada Joshi[3] · Saulius Juodkazis[4,18] · Olga Korotkova[19] · Kaupo Kukli[3] · Judy Kupferman[6] · Praveen Kumar[20] · Ravi Kumar[5] · Vijay Kumar[7] · Gokul Manavalan[6] · Ayush Mehra[6] · Naveen K. Nishchal[21] · Takashige Omatsu[2,26,27] · Cade Peters[13] · Andra Naresh Kumar Reddy[22,23] · Salla Gangi Reddy[5] · Valeria Rodríguez-Fajardo[24] · Carmelo Rosales-Guzmán[25] · Joseph Rosen[6] · Sarita[16] · Allarakha Shikder[21] · Rakesh Kumar Singh[16] · Xinzhou Su[12] · Aile Tamm[3] · Ganesh Velagala[5] · Petr Viewegh[8,9] · Eulàlia Puig Vilardell[3,4,18] · Alan E. Willner[12] · Agnes Pristy Ignatius Xavier[6] · Amit Yadav[16] · Huibin Zhou[12]

✉ Ganesh M. Balasubramaniam
balasubramaniam.gm@ntu.edu.sg

[1] School of Electrical and Electronic Engineering, Nanyang Technological University, 50 Nanyang Avenue, Singapore 639798, Singapore

[2] Molecular Chirality Research Center, Chiba University, 1-33, Yayoicho, Inage-ku, Chiba-shi, Chiba, Japan

[3] Institute of Physics, University of Tartu, W. Ostwaldi 1, 50411 Tartu, Estonia

[4] Optical Sciences Center and ARC Training Centre in Surface Engineering for Advanced Materials (SEAM), School of Science, Computing and Engineering Technologies, Optical Sciences Center, Swinburne University of Technology, Hawthorn, Melbourne VIC 3122, Australia

[5] Department of Physics, SRM University AP, Guntur, Andhra Pradesh 522240, India

[6] School of Electrical and Computer Engineering, Ben-Gurion University of the Negev, 8410501 Beer-Sheva, Israel

[7] Department of Physics, National Institute of Technology Warangal, Hanamkonda, Telangana 506004, India

[8] Institute of Physical Engineering, Faculty of Mechanical Engineering, Brno University of Technology, Technická 2, 616 69 Brno, Czech Republic

[9] Central European Institute of Technology, Brno University of Technology, Purkyňova 656/123, 612 00 Brno, Czech Republic

[10] Department of Optics, Palacký University, 17. listopadu 1192/12, 771 46 Olomouc, Czech Republic

[11] Department of Applied Physics & Science Education, Eindhoven University of Technology, Eindhoven 5612 AP, The Netherlands

[12] University of Southern California, Los Angeles 90089, USA

[13] School of Physics, University of the Witwatersrand, Johannesburg, South Africa

[14] Institute for Digital Molecular Analytics and Science, 59 Nanyang Drive, Singapore 636921, Singapore

[15] Laser Research Center, Physics Faculty, Vilnius University, Sauletekio Ave. 10, 10223 Vilnius, Lithuania

[16] Laboratory of Information Photonics and Optical Metrology, Department of Physics, Indian Institute of Technology (Banaras Hindu University), Varanasi 221005, India

[17] Department of Physics and Optical Science, University of North Carolina at Charlotte, Charlotte, NC 28223, USA

[18] Tokyo Tech World Research Hub Initiative (WRHI), School of Materials and Chemical Technology, Tokyo Institute of Technology, 2-12-1 Ookayama, Meguro-ku, Tokyo 152-8550, Japan

[19] Department of Physics, University of Miami, 1320 Campo Sano Ave, Coral Gables, FL 33146, USA

[20] Department of Physics, Indian Institute of Technology Bhilai, Kutelabhata, Bhilai, Chhattisgarh 491001, India

[21] Department of Physics, Indian Institute of Technology Patna, Bihta, Patna, Bihar 801106, India

[22] Laboratory of Nonlinear Optics, Institute of Astronomy, University of Latvia, Jelgavas 3, Riga LV-1004, Latvia

[23] Quantlight and High Harmonics Lab Pvt. Ltd., Door No. 304, Survey No. 30/P, Street No. 16, Nalanda Nagar, Hyderguda, 500048 Hyderabad, India

[24] Departamento de Física, Universidad Nacional de Colombia Sede Bogotá, Carrera 30 No. 45-03, Bogotá, Colombia

[25] Centro de Investigaciones en Óptica, A.C., Loma del Bosque 115, Colonia Lomas del Campestre, 37150 León, Guanajuato, Mexico

[26] National Yang Ming Chiao Tung University, No.1001, Daxue Road, East District, 300093 Hsinchu City, Taiwan

[27] Serendip Research Laboratory, 1-1-3-267, Umeda, Kita-ku, Osaka-shi, 530-0001 Osaka, Japan